Finite Element Guidelines for Simulation of Delamination Dominated Failures in Composite Materials Validated by Case Studies

Abstract The focus of this paper is on the computational modelling of progressive damage in composite structures of fibre reinforced laminae. A general review of modelling approaches to failure in the context of the finite element method is first presented, with an emphasis on models based on continuum damage mechanics. The way in which delamination and matrix splitting (that may or may not interact with fibre-tension damage) should be addressed in the framework of a commercial finite element code is considered next. An important feature of the analysis is it does not rely on customized user-subroutines but solely on the analysis capabilities of the general purpose software Abaqus, thus ensuring that the numerical results can be universally reproduced. It is shown that the finite element simulations can accurately represent the physical mechanisms controlling damage development and progression and reproduce a number of phenomena including delamination, laminate in-plane failure and behaviour at notches. The paper ends giving guidelines for the generalized modelling methodology using Abaqus without user-subroutines.

Keywords Delamination; Finite element modelling; In-plane failure; Notched strength.

1 Introduction

Composite structures commonly found in aerospace, automotive and civil engineering applications exhibit a distinctively nonlinear behaviour. This nonlinearity can arise in various ways. The heterogeneous nature of the material, which consists of fibres of one material (usually carbon or glass) in a matrix material of another (typically a polymer resin), makes the mechanical behaviour complex. This observation holds with respect to the stress-strain constitutive response, with directionally dependent properties, and to the failure behaviour, usually of a brittle type. In addition, since many composite structures consist of thin plates, they are likely to undergo large deflections.

The description of real composite behaviour is a challenge, either using experimental procedures, or numerical methods. In this respect, virtual tests for composite materials carried out by means of numerical modelling are increasingly replacing some mechanical and physical tests to predict and substantiate their structural performance and integrity due to recent developments in software-based nonlinear finite element analysis methods, particularly in composite-specific tools. This includes the computational advances in fracture modelling, especially the improvement of cohesive models of fracture and the formulation of hybrid stress-strain and traction-displacement models that combine continuum and discrete material damage representations in one single calculation.

Finite element simulations as virtual tests can be performed at any scale level of the structural composite. Fig. 1 illustrates a composite laminate with unidirectional plies and the three different modelling scales: (i) the microscale (constitutive modelling of fibre and matrix), (ii) the mesoscale (ply level as a multiphase material), and (iii) the macroscale (the laminate is modelled as a series of stacked unidirectional plies). In this contribution, modelling is performed on the mesoscale at which the ply is considered to be a homogeneous continuum. In other words, the material is homogenized by smearing the behaviour of the fibres and the matrix over a single ply. Interface elements between plies serve as the basis to model delamination.

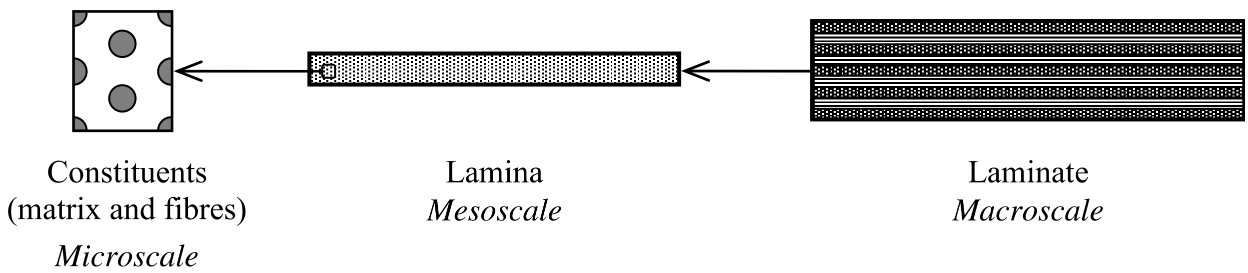

Fig. 1 Modelling scales for laminates

In order to obtain meaningful and reliable finite element simulations, the analysis has to account for the different failure (or damage) processes, mitigation, progression and their interaction. Matrix-dominated processes, especially delaminations, correspond to the onset of damage in most composite designs, and are one of the characteristics that distinguish their behaviour from that of metallic structures. Delamination can occur during manufacturing or due to interlaminar stresses, combined with a typically low through-thickness strength. Delaminations are often seen to occur at stress free edges due to the mismatch in properties of the individual plies, sections with thickness variation, at regions subjected to out-of-plane loading, and at notches. The introduction of notches to composite systems leads to stress concentrations that cannot be redistributed by plastic flow as in ductile metals.

These damage initiation mechanisms do not necessarily lead to loss of structural integrity. Further load can be accommodated due to stress redistribution over the fibres. This introduces the concept of progressive failure (or damage) of the composite material. In this framework, the numerical models are based on critical stress/strain values that trigger failure initiation, critical energy release values or damage mechanics considerations that describe failure propagation, as explained later. As this process progresses from mesoscale and macroscale to a large composite structure, the result is a continuing weakening of the whole structure, up to the point where the structure can no longer carry more load. This process is highly nonlinear as it degrades the ply and the laminate stiffness and extends beyond damage initiation.

This paper focuses on the analysis of the crucial role of delamination in determining in-plane strength of laminates that frequently leads to premature initiation of failure. The current study has been broken down into the following sections:

- Section 2 reviews the main features of computational finite element modelling of failure of composite materials. This review is also intended to serve as a point of departure for those who wish to pursue the subject matter. Therefore it is designed to offer as comprehensive a coverage as possible of the current state-of-the-art in the subject.
- Section 3 is concerned with (i) the application of cohesive zone interface elements to model delamination, and (ii) the benchmark analysis of notched composite plates, using the commercial finite element software Abaqus [1]. We first study delamination failures in simple configurations such as Double Cantilever Beam (DCB) and End Notched Flexure (ENF) tests. Splitting and delamination failures (and their interaction with fibre-breakage) are modelled next in centre notched cross-ply laminates. The numerical models include a continuum damage approach to intralaminar failure modelling and a cohesive zone model to represent the delamination behaviour at the interfaces. A simplified procedure to ensure damage localization is proposed. It is shown that the proposed model clearly captures the tendency of matrix dominated failure to propagate in the fibre direction using a continuum modelling approach, without the need to explicitly model the cracks by means of interface elements as in the original works. When properly implemented, the proposed methodology is shown to ensure a large degree of objectivity with respect to finite element discretization, and, simultaneously it requires little or no modification to standard commercial finite element codes, such as Abaqus [1]. This latter aspect is particularly relevant to practising engineers in industry who are concerned with virtual testing related to structural integrity and damage tolerance of fibre reinforced polymers for safety critical structures.
- A summary of guidelines for analysis and conclusions are presented in Sections 4 and 5, respectively.

2 Failure Analysis in the Context of the Finite Element Method

The full behaviour of composite structures can be predicted with numerical finite element simulations. The numerical modelling of this type of problem in the elastic range is quite straightforward. However, the nature of failure initiation and progression to rupture, involving matrix, fibre and/or interface damage and fracture, makes the analysis rather complex. Loads in composite structures are predominantly carried by axial forces in the fibres, and the failure process is driven by the energy released as they are unloaded after fracture. As well as this occurring by fibres failing, it can also happen by matrix dominated failures, in the form of cracks and delamination, joining-up to produce a fracture surface without the need to break reinforcing fibres.

The typical constitutive behaviour is characterized by an initial linear response followed by a second nonlinear phase of reduced stiffness that involves the formation of micro-cracks in the vicinity of the crack tip. The strain energy accumulated in the material specimen is released at the peak-load and a stable crack propagates progressively with a reduction in strength and stiffness until it eventually breaks. This is a typical quasi-brittle behaviour, although most polymer based matrices can deform plastically before damage when subjected to shear loading. This progressive damage modelling is carried out in three steps [2]:

1. Stress analysis: the geometry of the structure being known, together with the history of loading and initial conditions, the fields of stress and strain are first calculated by means of strain constitutive equations and a numerical procedure, e.g. finite element modelling.
2. Failure criterion or criteria: the most critical location(s) with regard to fracture is (are) determined and, the load corresponding to a macro-crack initiation at that point is calculated by integration of damage constitutive equations for the history of local stress or strain.
3. Degradation of material properties based on damage progression models to calculate the evolution of that macro-crack up to the final rupture of the whole structure.

This section reviews the main features of computational finite element modelling of failure of composite laminated structures. Some of the key concepts are considered first, including the element types and the material parameters. The mechanisms by which composites may fail are then discussed, first for intralaminar failure, and then for interlaminar delamination. The different approaches for the modelling of such mechanisms are also considered. Numerical aspects to the effective application of the progressive damage modelling are finally discussed.

2.1 Key Concepts

2.1.1 Element Types

An efficient geometric modelling has to account for the non-homogeneous and layered nature of the laminate. The finite element model must firstly represent the ply (or lamina) orientation, the stacking sequence and thickness variation, and secondly provide an adequate representation of the global stress field, the through-thickness stress variations, local stress concentrations and failure modes. The analysis has then to be treated as being three-dimensional. Solid (brick) elements with one layer of bricks representing each ply can be used. This option is not practical because the analysis would be computationally expensive to run if the layup had just more than a few plies. Additionally, conventional solids show an overly stiff behaviour and different effects of locking, especially the Poisson thickness locking effect, when used in very thin applications [3]. In practice, it is usual to employ shell elements, particularly in the form of *continuum shells*, which are elements that have the geometry of bricks but their kinematic and constitutive behaviour are similar to those of conventional shell elements. The continuum shell elements are able to reproduce reliable results in simulations of thin-walled structures by means of only one element over the thickness due to a higher-order displacement field. First approaches of this kind assumed a constant strain field over the thickness and can be found in Parisch [4], and Hauptmann and co-workers [5,6]. This approach was later extended by Remmers *et al*. [7] who considered an additional set of internal degrees of freedom to add a quadratic term to the displacement field that allows for a linear variation of the strain field over the thickness.

There are displacement and stress field singularities due to combined material/geometrical discontinuities between plies where intralaminar stresses develop during thermo-mechanical loading. This can lead to discrete delamination failures. This type of failure can be physically captured by means of a cohesive zone approach. Cohesive interface elements are currently adopted as a way of modelling this type of phenomenon [8-15]. In this approach, the discontinuous displacement field is described by *relative displacements* or *relative jumps* between a double set of nodes, for the normal (opening) and the two shear modes (sliding and tearing) [16]. An important feature of interface elements is that they include the effect of first failure, and the subsequent fracture propagation by means of critical strain energy release ratios. The interface layer is usually considered to be of zero (or nearly zero) thickness for analysis purposes.

2.1.2 Material Parameters

The unidirectional ply is an orthotropic material whose planes of symmetry are parallel and transverse to the fibre direction. The material coordinate axes are quite often designated as 1, 2 and 3, see Fig. 2:

- Axis-1 runs parallel to the direction of the fibres (longitudinal direction).
- Axis-2 runs normal to axis-1 in the plane of the ply (in-plane transverse direction).
- Axis-3 runs normal to the plane of the ply (through-thickness direction).

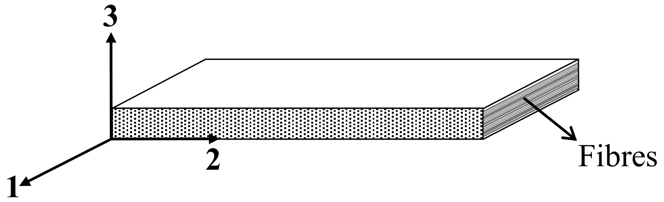

Fig. 2 Ply coordinate system

The mechanical behaviour of the materials in both continuum and interface modelling approaches is characterized by means of a constitutive law that includes the fundamental parameters. Damage-based material models for composite materials usually contain:

1. A law for the elastic behaviour of the elementary ply, which is idealized as a homogeneous material by smearing the distinct properties of the fibre and matrix, based on the transversely isotropic version of Hooke's law [17]. The relevant engineering constants are the moduli of elasticity in the fibre and transverse directions, E_1 and E_2, the longitudinal and transverse Poisson's ratios, ν_{21} and ν_{23}, the longitudinal and transverse shear moduli, G_{12} and G_{23}.
2. Longitudinal, transverse and shear strength of the lamina [18]:
   - $f_{1,T}$: axial strength in tension;
   - $f_{1,C}$: axial strength in compression;
   - $f_{2,T}$: transverse strength in tension;
   - $f_{2,C}$: transverse strength in compression;
   - $f_{1,S}$: shear strength in the axial direction;
   - $f_{2,S}$: shear strength in the transverse direction.
3. Fracture energy (or fracture thoughness), G_c, in the above directions [19-21]. G_c governs crack growth and is defined as the work needed to create a unit area of a fully developed crack.

The interface behaviour is represented by cohesive laws, first introduced by Dugdale [22] and Barenblatt [23] in the context of the problem of equilibrium cracks. These constitutive relations describe the stress-separation behaviour (also known as the cohesive traction versus jump displacement law) of a failure process zone. In fracture mechanics, any cohesive law consists of three main features that are identical to the above:

1. An elastic region characterized by a scalar stiffness parameter, which can be interpreted as a penalty factor.
2. The interfacial strength.
3. The area enclosed by the traction-displacement curve that is equal to the fracture toughness of the material.

The shape assumption of the curve completes the cohesive law. Although a variety of geometric shapes have been proposed (e.g. Tvergaard and Hutchinson [24], Xu and Needleman [25], who proposed trapezoidal and exponential laws, respectively), the simple bi-linear curve representation (e.g. Mi *et al*. [8], Camanho *et al*. [26], Jiang *et al*. [14]) is usually implemented for modelling the cohesive behaviour. Finally, a clear distinction between the possible failure modes of the interface (see Fig. 3), opening (mode I), sliding (mode II) and tearing (mode III) has to be made as each mode is associated with distinct values for strength and fracture toughness. In practice, modes II and III are not easily dissociated and therefore the same interfacial strength and fracture energy are adopted in computational analysis.

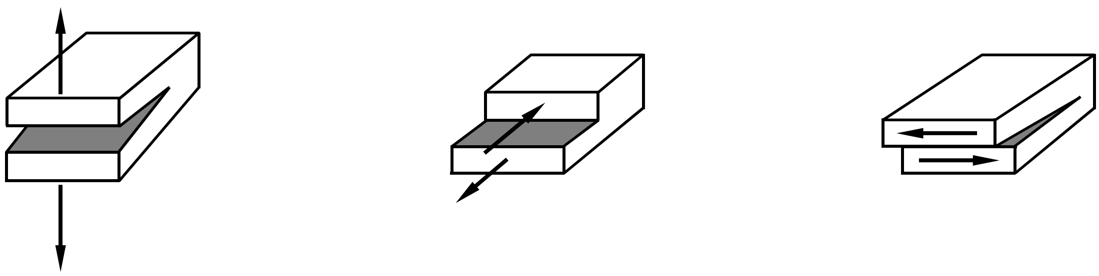

a) Mode I: opening **b)** Mode II: sliding **c)** Mode III: tearing

Fig. 3 Modes of delamination failure

2.2 Intralaminar Failure Modelling

The intralaminar failure mechanism of a composite material is characterized by matrix cracks that run parallel to the fibres and propagate through the thickness of the laminate, rather than the laminae, shear in transverse or longitudinal directions, and fibre breaking cracks, as can be seen in Figs. 4a-c [27]. Matrix failure mechanisms are usually the first form of damage observed in laminates. Fibre fracture marks the ultimate failure in a well-designed laminate. In fact, fibre fracture can be seen as the *only desirable* fracture mechanism, since the fibre reinforcement forms the main load carrying structure. In Figs. 4a and 4b the fracture surfaces caused by transverse compression and transverse shear respectively are illustrated too. The fracture angle ±35° to ±40° is typical for pure compression [28]. The fracture angle for pure transverse shear is approximately 45°. This fracture behaviour is well known for brittle materials.

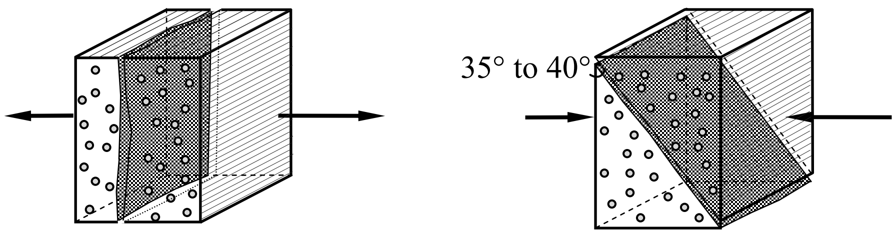

Transverse tension (mode 2,T)   Transverse compression (mode 2,C)

a) Matrix failure

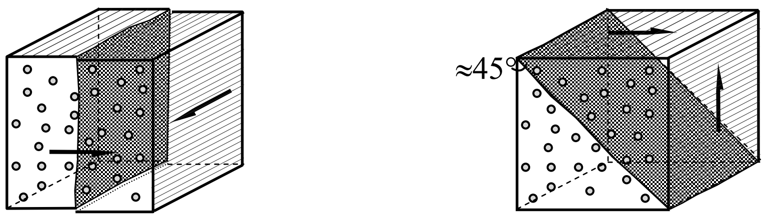

Transverse shear (mode 2,S)   Longitudinal shear (mode 1,S)

b) Shear failure

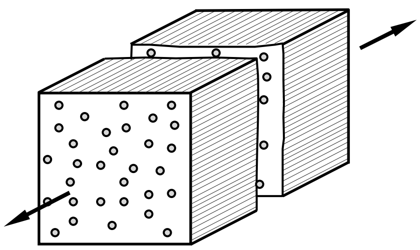

Fibre breakage

Tension (mode 1,T)

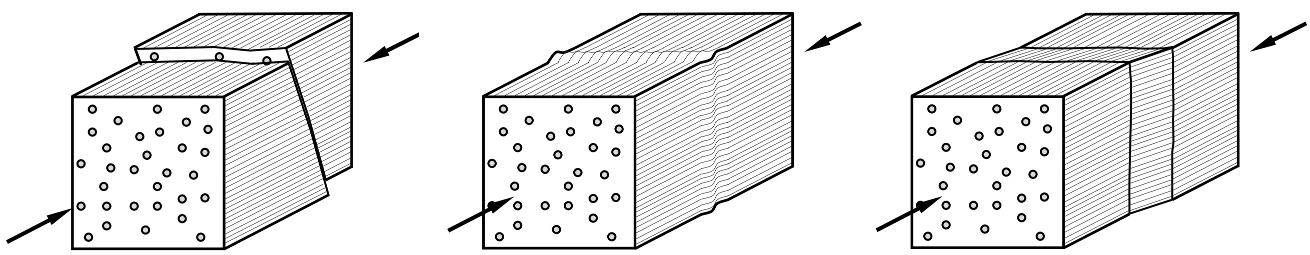

Fibre fracture in shear   *Micro-buckling*   *Kinking*

Compression (mode 1,C)

c) Fibre failure

Fig. 4 Forms of failure (after Knops [27])

Continuum damage mechanics models for the prediction of intralaminar failure are used in this work with a range of examples on different applications. The damage mechanics of composites is the modelling of the initiation and degradation phenomena at a structural analysis scale. At this scale, the laminate is modelled as a stacking of homogeneous layers connected by interfaces. Relative variations of stiffness are the damage indicators. The progressive transverse matrix cracking and the brittle fracture of fibres are included at the single lamina level. The damage state at every (1,2) point, see Fig. 2, is assumed to be uniform within the layer thickness.

2.2.1 Failure Initiation Theories of a Lamina

Literature presents two types of failure initiation criteria for a lamina: phenomenological and physically-based. Phenomenological criteria have been proposed by extending and adapting failure theories to account for the anisotropy in stiffness and strength, but they do not reflect the level of complexity that is inherent to this type of structural material. Underlying such complexity is the fact that composites consist of mechanically dissimilar phases, stiff elastic brittle fibres and a compliant yielding matrix. Physically-based criteria distinguish between states of stress not leading to fracture and those implying fracture.

The Tsai-Wu interactive (phenomenological) criterion [29] is the most commonly adopted in research methodologies and essentially consists of a single relation for the interaction of the different internal stress components σ_i in the material frame. For a general anisotropic material the failure surface in the stress-space has the following scalar form:

$$F_i\sigma_i + F_{ij}\sigma_i\sigma_j = 1 \quad \text{and} \quad F_{ii}F_{jj} - F_{ij}^2 \geq 0 \tag{1}$$

whereby F_i, F_{ij} are strength tensors of the second and fourth rank, respectively. The following contracted notation is used in the above equation: $i, j = 1, 2, \ldots 6$.

The first failure theory that makes a clear distinction between the different lamina failure modes was developed by Hashin and Rottem [30], later modified by Hashin [31] to predict the onset of damage. This theory consists of the following expressions:

Fibre in tension $\dfrac{\sigma_1}{f_{1,\mathrm{T}}} = 1$

Fibre in compression $\dfrac{\sigma_1}{f_{1,\mathrm{C}}} = 1$

Matrix in tension $\left[\dfrac{(\sigma_2+\sigma_3)^2}{f_{2,\mathrm{T}}^2} + \dfrac{\tau_{23}^2 - \sigma_2\sigma_3}{f_{2,\mathrm{S}}^2} + \dfrac{\tau_{31}^2+\tau_{12}^2}{f_{1,\mathrm{S}}^2}\right]^{\frac{1}{2}} = 1$ (2)

Matrix in compression $\left[\left[\left(\dfrac{f_{2,\mathrm{C}}}{2f_{2,\mathrm{S}}}\right)^2 - 1\right]\dfrac{\sigma_2+\sigma_3}{f_{2,\mathrm{C}}} + \dfrac{(\sigma_2+\sigma_3)^2}{4f_{2,\mathrm{S}}^2} + \dfrac{\tau_{23}^2 - \sigma_2\sigma_3}{f_{2,\mathrm{S}}^2} + \dfrac{\tau_{31}^2+\tau_{12}^2}{f_{1,\mathrm{S}}^2}\right]^{\frac{1}{2}} = 1$

whereby σ_i and τ_{ij} (i, j = 1,2,3) are the principal stresses for the lamina. The failure criterion used to predict matrix tensile and compressive cracking includes the shear stresses that may lead to matrix shear failure, as can be seen in Eqs. (2c-d). The Hashin criterion is used in this research work to predict damage onset and governing failure mode within a ply. This criterion has been shown by many researchers to be easily implemented in finite element analyses and requires lamina properties that can be fairly easily determined on an experimental basis. Furthermore, it has provided numerically reliable results when applied to predict the *first ply failure load* in both carbon fibre and glass fibre composite materials. In most cases, the laminate can carry greater loads because it possesses damage tolerance prior to complete rupture. It is often the case that a sequence of ply failures occurs under increasing stresses before final rupture of the whole laminate.

2.2.2 Damage Progression Models

For composite structures that can accumulate damage, the use of failure initiation criteria is not sufficient. The rate and direction of damage propagation defines the damage tolerance of the structure and its final damage state. Consequently, once a failure initiation criterion is satisfied, the associated damage variable is different from zero and further loading will cause degradation of the material stiffness coefficients. The major challenge is to choose appropriate combinations of failure criteria and degradation models. These models can be divided into two main groups:

- Heuristic models based on a ply-discounting material degradation approach [32,33].
- Serial / parallel mixing models based on compounding nonlinear constitutive relationships [34-37].
- Progressive failure models based on continuum damage mechanics [21,38-43].

The classical ply discount method assumes that a failed ply cannot take any further load. In reality, a fractured ply can exhibit significant load-carrying capacity. In addition, delamination damages are not taken into account by ply discount methods.

Serial / parallel mixing models are able to predict the failure and post-failure behaviour of laminates. These models can be understood as constitutive equations managers that obtain the composite constitutive performance by combining the mechanical behaviour of its different constituents, i.e. matrix and fibres [35]. These models are able to simulate both intralaminar [34,35] and interlaminar [36,37] failures by means of continuum mechanics.

The basic approach of progressive failure analysis is to assume that all material nonlinearity is due to damage in the form of reduced stiffness. Accordingly, the majority of existing models for progressive intralaminar failure analyses are based on softening constitutive models that use (i) scalar damage variables, or (ii) mode-specific strain energy release rates (fracture toughness) and total dissipated strain energy [40,44-46]. Displacements due to crack opening are smeared over a characteristic element, as defined in Section 2.4. The shape of the softening law is often assumed to be inconsequential for the prediction of fracture, provided that it is defined as a function of the fracture toughness [47].

The approach used in this research work is based on the energy requirement for the deterioration of stiffness within a characteristic or unit volume per unit time. It also assumes that the strain energy dissipates gradually as damage develops. Damage evolution laws are defined for the various possible failure modes (Fig. 4). Each damage evolution law includes the corresponding fracture toughness, representing the energy dissipated by inelastic processes in the fracture process zone. Guidelines for the computation of these values are summarized in [21] and [42].

2.2.3 Simulation of Progressive Damage in Abaqus

The present continuum damage model in Abaqus predicts the onset and accumulation of intralaminar damage mechanisms, as well as final structural collapse by the propagation of a macro-crack. For this modelling, the Hashin criteria are used for damage initiation, see Eqs. (2). The influence of damage on the constitutive model is based on the work of Matzenmiller *et al*. [39]. A drawback of this damage progression model is that it does not reproduce localization of tensile fracture properly. This aspect is of concern, and will be resolved by means of the crack band approach, initially developed by Bažant and Oh [48]. The *crack band model* uses a modification of the post-peak part of the constitutive law (damage progression) to enforce the energy dissipation as determined by experiments by a localized crack band. This simple approach will be further detailed in Section 2.4.

2.3 Interlaminar Delamination Modelling

The fibre-matrix interface gives composites their structural integrity. The interface consists of the bond between fibre and matrix and the immediate adjacent region. The load transfer from the matrix to the fibre that takes place at the interface layer is primarily a mechanistic process and involves the interfacial bond and friction. Delamination is defined as the separation of layers from each other, as a consequence of shear stresses acting in planes parallel to the layers interfaces and/or tensile stresses acting in the through-thickness direction. This phenomenon is a typical *crack growth* problem and is treated in the framework of fracture mechanics. Today, the most popular computational method for the prediction of delamination between plies in laminated composites is based on *cohesive zone models* that provide a natural bridge between strength-based models and energy-based models for fracture, allowing delamination to be described by a single framework that covers a range of applications for which the strength or energy criteria alone might not be sufficient. Cohesive zone models describe highly localized inelastic processes by traction-separation laws that link the cohesive traction transmitted by a discontinuity line or surface to the displacement jump, characterized by the separation vector [49-51]. Independent cohesive laws are used for the opening mode I, and the sliding and tearing modes, II and III, i.e. the toughness and interfacial strength values for the three modes are different. Following the approach of Yang and Cox [52], the same cohesive law can be assumed for the shear modes II and III.

The simulation of interlaminar damage will be based on the cohesive zone approach using the Abaqus three-dimensional cohesive element COH3D8 at the plies interfaces. The study is performed in quasi-static regime. The traction-separation law formulation assumes a nonzero elastic stiffness of the cohesive zone, which is physically motivated by the reduced stiffness of the matrix rich interface layer as compared to a perfect bond between matrix and fibres. From a numerical point of view, this elastic stiffness can be understood as a penalty-type enforcement of displacement continuity in the elastic range. Different guidelines have been proposed for selecting the stiffness of the interface. Daudeville *et al*. [53] calculated the stiffness in terms of the thickness and the elastic modulus of the interface. Camanho *et al*. [26] used a fixed value of 10^6 N/mm^3 for the modelling of graphite fibre/epoxy matrix laminates, which is a numerical parameter large enough to ensure the displacement continuity at the interface. Turon *et al*. [54] proposed the following relationship:

$$K = \alpha E_3 / t_{\max} \tag{3}$$

whereby α is a coefficient ($\alpha >> 1$), and $t_{\max}$ is the larger of the sub-laminate thicknesses above or below the cohesive layer. The choice of the coefficient α has to account for the adverse effect that relatively large stiffness values have (i) on the conditioning of the global stiffness matrix for implicit methods, and (ii) on the critical time step for explicit methods. In order to satisfy these requirements, Turon *et al*. [54] proposed a α value of 50.

A quadratic stress criterion is used for the damage initiation criterion, i.e. to specify the conditions for separation in the cohesive zone model [26,55,56] and can be expressed as follows:

$$\left(\frac{\langle\sigma_{\mathrm{n}}\rangle}{f_{\mathrm{I}}}\right)^2+\left(\frac{\sigma_{\mathrm{s}}}{f_{\mathrm{II}}}\right)^2+\left(\frac{\sigma_{\mathrm{t}}}{f_{\mathrm{III}}}\right)^2=1 \tag{4}$$

whereby σ_{n} is the stress in pure normal mode, σ_{s} is the stress in the first shear direction, σ_{t} is the stress in the second shear direction, f_{I}, f_{II} and f_{III} are the peak strength values in the same directions, and:

$$\langle\sigma_{\mathrm{n}}\rangle=\sigma_{\mathrm{n}} \quad \text{for} \quad \sigma_{\mathrm{n}}>0 \qquad \text{and} \qquad \langle\sigma_{\mathrm{n}}\rangle=0 \quad \text{for} \quad \sigma_{\mathrm{n}}\leq 0 \tag{5}$$

because compressive normal stresses do not open the crack.

Progression of damage at the interfaces is modelled using a linear softening law and a critical mixed mode energy behaviour based on the Benzeggagh-Kenane criterion [57], which is expressed by the following expression:

$$G_{\mathrm{c}}=G_{\mathrm{I,c}}+\left(G_{\mathrm{II,c}}-G_{\mathrm{I,c}}\right)\left[G_{\mathrm{II}}/\left(G_{\mathrm{I}}+G_{\mathrm{II}}\right)\right]^{\eta} \tag{6}$$

whereby $G_{\mathrm{m,c}}$ (m = I, II, III) is the total critical strain energy release rate associated with delamination mode m, and η is the semi-empirical criterion exponent applied to delamination initiation and growth.

2.3.1 Numerical Aspects of Cohesive Zone Modelling

In the cohesive zone modelling framework, implemented in Abaqus, two parameters are needed: the interfacial strength and the energy release rate, which control delamination initiation and propagation, respectively.

The use of cohesive zone models in finite element analyses requires that a very fine mesh is used to ensure that enough interface elements exist within the cohesive zone length at the crack tip. If the mesh is too coarse, the cohesive stress at the discontinuity may not even reach the interfacial strength and, as a result, failure is missed. Falk *et al.* [50] suggest a minimum of two to five elements in order to perform a reliable simulation. To have an idea of the figures involved, Turon *et al.* [54] indicate that for typical graphite-epoxy or glass-epoxy composite materials, the length of the cohesive zone should be smaller than one or two millimetres. As a consequence, the mesh size required in order to have more than two elements in the cohesive zone should be smaller than half a millimetre. For large structural models this has the obvious consequence of a computational expensive solution.

To overcome this problem, it is common practice to use interfacial strength values that are lower than those determined experimentally [54,58] whilst maintaining the same fracture toughness, see Fig. 5. This procedure is based on an artificial increase of the cohesive zone length by reducing the interfacial strength and keeping the energy release rate constant. While the implications of this procedure have been discussed in literature for the finite element analysis of DCB and ENF specimens, which are designed to produce pure normal mode I and pure shear mode II delamination, respectively, without any intralaminar material damage, this method has been also applied in many other instances in which delamination interacts with matrix splitting.

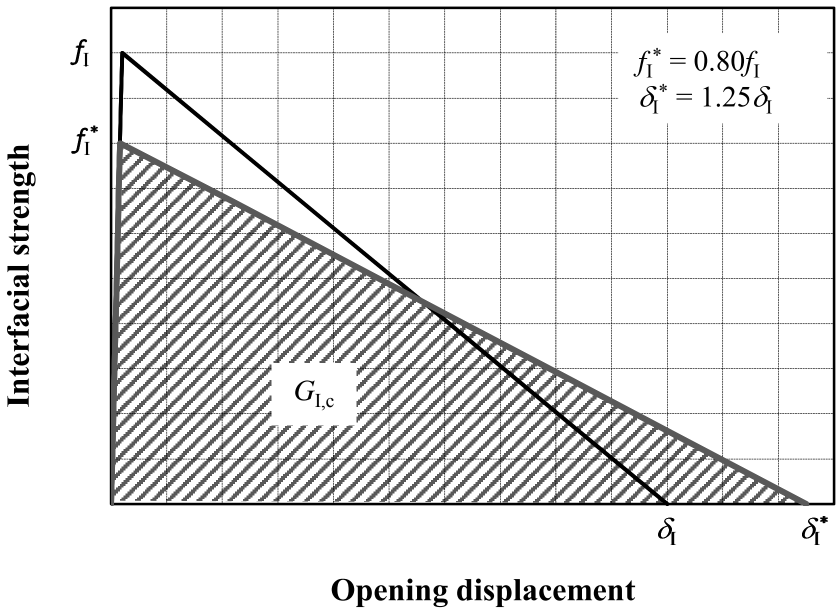

Fig. 5 Bi-linear traction-separation response (particular case: curve for mode I): variation of interfacial strength

2.4 Regularization in Quasi-Static Regime

The underlying mathematical problem of damage-induced deformation localization is that of an ill-posed boundary-value problem, i.e. a system of ordinary differential equations with solution and derivative values specified at different points. In general, numerical methods for analysing and solving ill-posed problems include a so-called *regularization parameter*, which controls the degree of smoothing (or regularization) applied to the problem. The technique involves a mathematical scheme called *localization limiter*, in order to avoid *size effect* and *numerical instability*.

Failure occurs by progressive damage that involves strain localization processes that result in a sharp decrease of the load-carrying capacity. Strain localization is a concept that describes a deformation mode, in which the whole deformation of a structure (made from a specific material) occurs in one or more narrow bands, referred to as the fracture process zone. The formation of these bands is accompanied by a softening response, usually leading to complete collapse. The width and direction of localization bands depend on the material parameters, geometry, boundary conditions, internal stresses/strains, loading distributions and loading rate. As a consequence, numerical predictions using continuum damage mechanics are found to be strongly dependent on the size of the finite element mesh. This problem is known as *spurious mesh sensitivity*: the energy that is released by cracking damage depends on the mesh size and tends to zero in the limit of an infinitesimally refined mesh. The explanation for this phenomenon is rather trivial. The release of stored energy into the fracture front, as described by the *local* stress-strain relationship per unit volume, tends to zero when the length of the crack tends to zero. To overcome this difficulty, the material constitutive model has to be supplemented with some mathematical condition that prevents localization of smeared cracking into arbitrarily small regions [59]. *Nonlocal* damage theories have emerged as an effective means for capturing the size effects. These theories basically relate the stress at any point to the state of deformation within a finite volume about that point [51,60,61]. The simplest, and computationally most effective, type of nonlocal approach is the *crack band model* [48]. The model ensures the correct energy dissipation in a localized damage band by rescaling the energy of the post-localization part of the stress-strain relationship by taking the size of the finite elements into account [51]. The crack band model provides only a *partial regularization* of the problem, i.e. it is not a true localization limiter, as it allows the global response characteristics to be truly captured, but the width of the numerically resolved fracture process zone is still dependent on the mesh density [62]. In this context, Bažant and Oh [48] derived the following critical size l^* (element characteristic length or length of the fracture process zone) by adjusting the energy dissipated by each failure mechanism M:

$$l^* \leq \frac{2E_{\mathrm{M}}G_{\mathrm{M,c}}}{f_{\mathrm{M}}^2} \tag{7}$$

whereby E_{M}, $G_{\mathrm{M,c}}$ and f_{M} are the relevant modulus of elasticity, fracture energy and strength, respectively. The authors suggest a practical critical size of about half of that determined from Eq. (7).

The crack band model performs best if the path of the fracture process zone is known in advance (e.g. tension failure of open hole laminates loaded in tension), and if the mesh is designed to coincide with this zone.

Strain-softening constitutive models cause additional convergence problems when using global solution methods because the tangential matrix of the softening material ceases to be positive definite. This leads to lack of robustness within the equilibrium iterations. The *numerical instabilities* can be prevented by adding *viscosity* to the constitutive model (rate-dependent behaviour). The *artificial viscosity regularization* leads to corresponding stiffness matrices that shall guarantee stable equilibrium iterations. This approach was first proposed by Needleman [63] to overcome this type of problem when analysing fracture processes in metals. Needleman also showed why introducing viscous terms in damage laws could be a convenient way to regularize the ill-posed problems of rate-independent laws.

In this contribution, the general framework of viscous regularization is adopted, as recommended by Abaqus with its composite damage model, although it involves a nonphysical rate dependence, and consequently additional effort in model calibration and validation. Values for this parameter are generally determined by using inverse modelling techniques because it cannot be explicitly related to any physical quantity. Both Lapczyk and Hurtado [41] and Maimí *et al*. [64] successfully implemented artificial viscosity in their continuum material models to improve the convergence of the numerical algorithm. Chaboche *et al*. [65], Gao *et al*. [66] and Hamitouche *et al*. [67] used viscous regularization to solve localization problems related to the application of the cohesive zone model.

2.5 Nonlinear Solution Process

The nature of a progressive failure methodology requires a nonlinear implicit or explicit solver to establish equilibrium. In implicit formulations, the current stress state and a consistent local tangent material stiffness matrix are needed to form the internal force vector for the residual force vector computation, to generate the Jacobian matrix, and to solve the set of algebraic equations at every time step using a Newton-Raphson-like method. In explicit formulations, only the current stress state is needed to evaluate the current internal force vector in order to advance the transient solution forward in time. Explicit solvers do not need to form a global stiffness matrix because the linear equations are not solved simultaneously for the entire system (like in implicit method), but the stress wave propagates element-to-element (local).

Abaqus implements both implicit (Abaqus/Standard) and explicit (Abaqus/Explicit) solvers. The implicit solution strategy is suitable for problems involving smooth geometric and material nonlinear analyses. The geometric nonlinearity is due to large strain and large rotation kinematics. The nonlinear material behaviour is due to the degradation of the mechanical properties of the laminae and the matrix rich layer between laminae to simulate intralaminar and interlaminar damage mechanisms. A load stepping routine is used in Abaqus/Standard. There is no restriction on the magnitude of the load step as the procedure is unconditionally stable. The increment size follows from numerical accuracy and convergence criteria. Within each increment, the equilibrium equations are solved by means of the Newton-Raphson method, which is stable and converges quadratically. In this method, for each load step, the residuals are eliminated by an iterative scheme. In each iteration, the load level remains constant and the structure is analysed with a redefined tangent stiffness matrix. The accuracy of the numerical solution is measured by means of appropriate convergence criteria. Their selection is of the utmost importance. Too tight convergence criteria may lead to an unnecessary number of iterations and a consequent waste of computer resources, whilst a loose tolerance may result in incorrect or inaccurate solutions. Generally speaking, in nonlinear geometrical analyses relatively tight tolerances specific to the problem are required, while in nonlinear material problems slack tolerances are admitted, since high local residuals are not easy to eliminate. Abaqus/Standard provides the option of including a *line search algorithm* [68] to improve the robustness of the Newton-Raphson method.

With respect to the incremental method, a load curve is defined. Loads should be applied to the specimen in a displacement-control fashion that enforces a better conditioning of the tangent stiffness matrix when compared to the classical load-control procedure.

Explicit schemes offer a more robust alternative for convergence for quasi-static load cases but may come at an even higher computational cost as smaller solution time steps are required, in addition to unwanted inertial effects. The time step must be less than a critical value based on the highest eigenvalue in the model. The stable time increment Δt_{stable} is the minimum time that a dilatational wave takes to move across any element in the model, and is given by:

$$\Delta t_{\text{stable}} = l^* \sqrt{\rho / E_1} \tag{8}$$

where ρ is the material density. The stable time steps for quasi-static explicit analyses are very small, of the order of 10^{-8} s or less, and the whole calculation process requires hundreds of thousands of increments. Mass scaling and damping are common approaches to assist in artificially reducing the computational time. Quality checks, such as the ratio of kinetic energy to internal energy have to be carried out to ensure that the problem is still essentially quasi-static. An acceptable rule of thumb is to set acceptance of this ratio to 0.01~0.05.

3 Benchmark Applications

The present section describes the finite element models developed in the current work. The models incorporate separate finite element types for laminae and interfaces to simulate damage evolution of combined intralaminar and delamination failures. The evolution of these two physical damage forms is strongly coupled. Experimental and numerical results available from literature on advanced composites are used for calibration and validation of the proposed models.

First, and for the purpose of trying to use experimental and numerical data to characterize cohesive material properties the DCB and ENF tests that isolate delamination behaviour are simulated.

Second, notched laminates under in-plane tensile loading are considered. Two cases are analysed: a laminate with a centre crack, and a double edged-V-notched laminate. These are challenging problems in composite materials because failure involves complex mechanisms such as fibre breakage, matrix cracking and delamination. In addition, the laminate strength and dominant failure modes can depend on geometrical parameters and material properties, such as notch dimensions, stacking sequence and ply thickness. The detailed matrix damage development at notches under tensile loading, in the form of matrix splitting cracks in the plies perpendicular to the notch, together with narrow triangular areas of delamination, is well captured by modelling laminates with sharp notches, as a centre crack, or a double edge-V-notch.

3.1 Delamination Fracture Testing

Numerical results on modes I and II fracture of glass fibre and carbon fibre unidirectional composites, using the DCB and ENF specimens, respectively, are presented in this section. Results are validated with experimental results published by Davidson and Waas [69] and Turon [13].

The basic configurations for the DCB and ENF test specimens are identical, as can be seen in Fig. 6. The only difference between the two is in how the load is applied. The specimen consists of a rectangular unidirectional laminate with uniform thickness, containing a nonadhesive insert at the midplane, which serves as a delamination initiator [70]. In the tests, the delamination between the two unidirectional plies will grow from the insert, which is the tip of the initial crack, to the other end of the specimen. To simulate the delamination smooth growth in these tests, cohesive elements are placed at the interface between the two plies in the finite element analyses. These elements are removed from the mesh when the released energy corresponds to the fracture energy of the material.

To provide a framework against which to assess the numerical formulation, this report includes a set of closed-form analytical load-displacement solutions that can be found in Mi *et al*. [8], Harper and Hallett [58] and Reeder *et al*. [71]. These are summarized below for completeness.

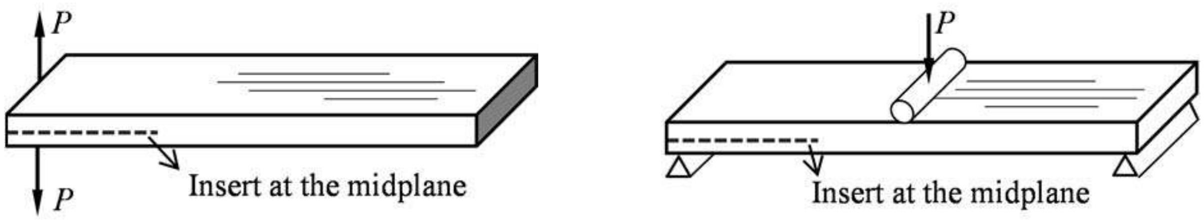

DCB ENF

Fig. 6 DCB and ENF specimens

3.1.1 Mode I Delamination

As a pure mode I problem, a glass fibre unidirectional composite DCB specimen is analysed under displacement control. The experimental setup of Davidson and Waas [69] is simulated. The geometry of the specimen and the boundary conditions are illustrated in Fig. 7. Although the nominal cantilever thickness t is 2.5 mm, the measured thickness values varied from a minimum of 2.3 to 2.7 mm. The initial length of the crack a_0 is 50 mm. The material data assumed for the finite element model are given in Table 1. For the laminate, Davidson and Waas [69] give elastic constants E_1 and ν_{12}. The remaining material properties were assumed to be those of a transverse isotropic material and were scaled relative to the value of E_1 [72]: $E_2 = E_1$, $G_{12} = G_{13} = E_1/18$ and G_{23}

$= E_1/31$, although a sensitivity analysis of the finite element model to the value of these parameters has shown their influence to be irrelevant. For the cohesive elements, the distribution of the critical energy release rate $G_{I,c}$ shows values ranging from a minimum of 1.5 N/mm to a maximum of 2.2 N/mm and a mean value of 1.8 N/mm. The single interface stiffness value for K_I, K_{II} and K_{III} were computed by means of Eq. (3).

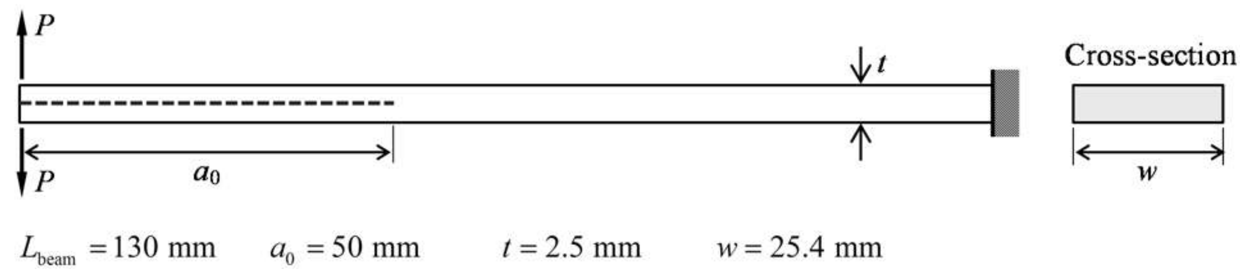

Fig. 7 DCB benchmark test coupon geometry (nominal dimensions)

Table 1 Material properties of the DCB specimen

Lamina properties		Interfacial properties			
			Mean	Min	Max
E_1 (N/mm^2)	11500	$G_{I,c}$ (N/mm)	1.8	1.5	2.2
E_2 (N/mm^2)	11500	$G_{II,c} = G_{III,c}$ (N/mm)	3.6	–	–
$G_{12} = G_{13}$ (N/mm^2)	640	f_I (N/mm^2)	13	–	–
G_{23} (N/mm^2)	370	$f_{II} = f_{III}$ (N/mm^2)	20	–	–
ν_{12}	0.3	$K_I = K_{II} = K_{III}$ (N/mm^3)	23000	–	–

The material properties set out in Table 1 deserve comment. The modulus of elasticity E_1 is relatively low for practical unidirectional glass fibre composites. Generally speaking, these type of laminates with 55%~60% of fibre volume content has $E_1 \approx 40000$ N/mm^2, which is approximately 3.5 times the value specified by Davidson and Waas [69]. Although the authors do not give an explanation for such an unusual value, a careful analysis of the glass composite laminates tested by the authors shows that the actual specimen is not an unidirectional laminate. It can be seen in the referenced paper that the laminae have 90° fibre reinforcement towards the outer surfaces in the thickness direction. The fibre bridging seen in the experiments can be for a unidirectional layer at the mid-plane of the laminate where the crack is forced to propagate. A value for E_1 of 11500 N/mm^2 can only be a real elastic modulus for the laminate if the unidirectional layer with 55%~60% of fibre volume content is a thin mid-plane core. There is a technical reason why the construction could be a three-layered sandwich having a biaxial reinforcement in the outer layers. If the laminate was purely unidirectional, it would be very fragile in handling to failure by longitudinal transverse splitting. This specimen was certainly prepared for the fracture toughness testing.

For the numerical analyses, a relatively fine mesh was adopted with 26520 linear shell continuum elements for the specimen of volume 8255 mm^3 with 2.5 mm thickness, with three integration points along the ply thickness, and 8160 cohesive elements for the interface. This mesh density was chosen from a mesh convergence study for the overall load versus crosshead displacement to ensure that the results of the analysis were not affected by changing the size of the mesh. Three convergence runs were performed with constant element sizes of 1 mm, 0.5 mm and 0.25 mm. It was found that the element side length of 0.5 mm enabled an accurate analysis of the global load versus displacement response and the cohesive zone stress distribution to be well captured. This appears consistent with previous mode I studies by Turon *et al*. [54]. An implicit finite element scheme with small displacement increments of 5×10^{-3} mm was used in the simulations. The comparison between numerical, experimental (three specimens, Sp. 1, 2 and 3) and analytical load versus crosshead displacement is given in Figs. 8 and 9. The actual experimental relationship is used to compute the mode I critical energy release rate $G_{I,c}$ whereas for the numerical and analytical analyses, this value of $G_{I,c}$ is input data to be able to obtain the load-deflection relationship.

Fig. 8a shows the numerical simulation results (generally labelled FE in the legend to graph) for the maximum, nominal and minimum values for the laminate thickness t and a fixed $G_{I,c}$ equal to the mean value in Table 1. It can be seen that the crack initiation point is not well captured and the post-initiation curve is severely under-predicted by 30% for nominal thickness. The elastic behaviour is reasonably predicted when the maximum thickness value is used. This finding potentially highlights the poor specification of the modulus of elasticity E_1. In Fig. 8b, the DCB thickness was fixed to the maximum value of 2.7 mm and the upper bound, mean and lower bound of the experimental $G_{I,c}$ were used. Simulations show similar elastic behaviour, i.e. prior to delamination initiation. The three post-initiation numerical curves run parallel but only the curve for $t = 2.7$ mm and $G_{I,c} = 2.2$ N/mm shows a good agreement to the experiments.

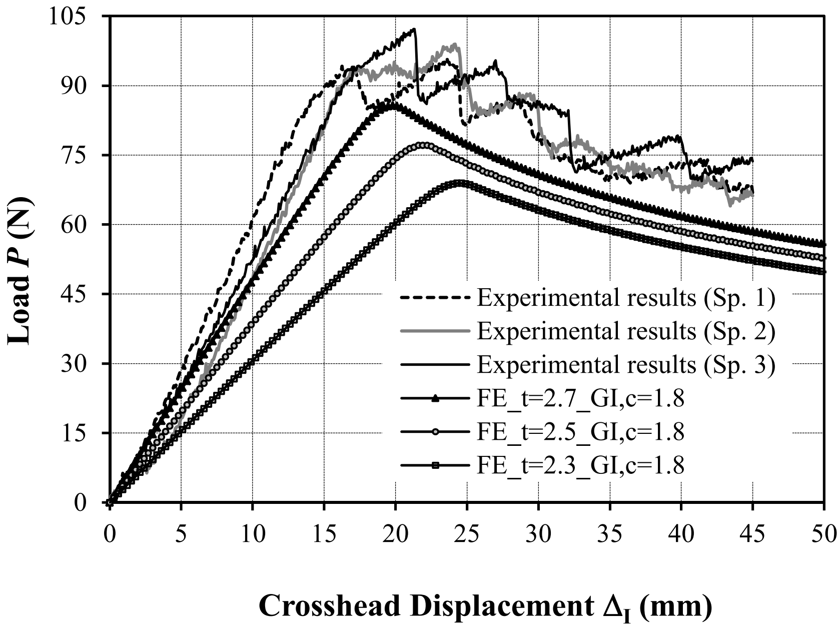

a) Variation in thickness

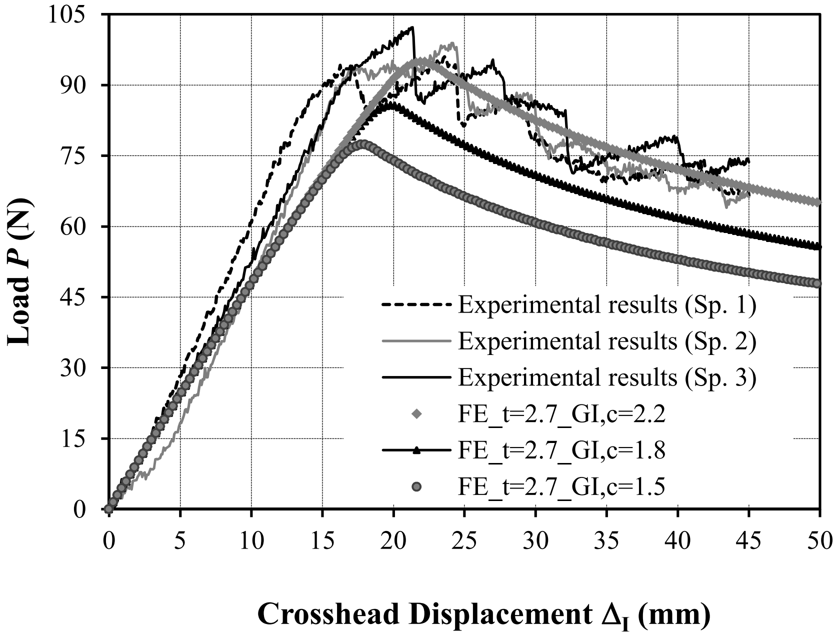

b) Variation in critical energy release rate

Fig. 8 Load versus crosshead displacement: comparison between experimental (three specimens, Sp. 1, Sp. 2, Sp. 3) and numerical results

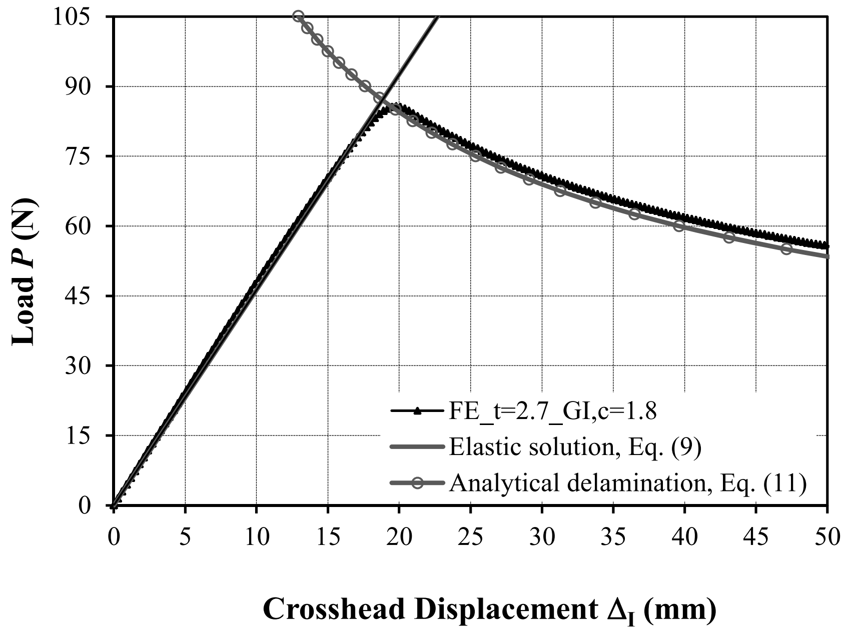

a) Maximum thickness of 2.7 mm

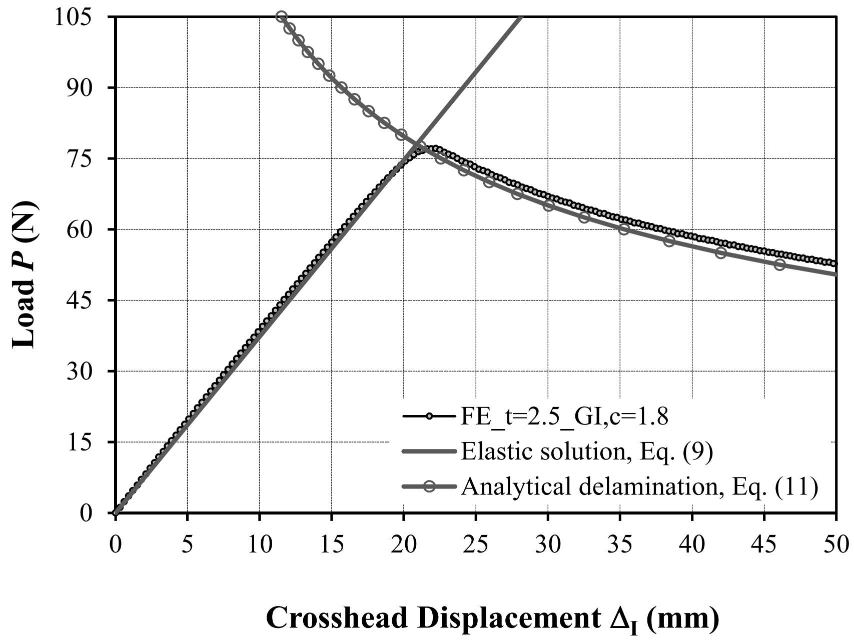

b) Nominal thickness of 2.5 mm

Fig. 9 Load versus crosshead displacement: comparison between analytical and numerical results using the mean value of critical energy release rate

The linear analytical solution for the DCB specimen, which is considered as two single cantilever beams is obtained from corrected beam theory that accounts for shear and local deformations. The linear vertical separation of the cantilevered beam tips (or crosshead displacement) Δ_I, is thus given by [58,71]:

$$\Delta_{\mathrm{I}} = \frac{2P\left(a_0 + \chi t\right)^3}{3E_1 I} \tag{9}$$

where P is the point load applied to the free end of each cantilever, a_0 is the initial crack length prior to crack propagation, I is the second moment of area of each cantilever ($I = wt^3/12$, w: width), and χ is a correction parameter, defined as:

$$\chi = \sqrt{\left[3 - 2\left[\frac{\Gamma}{\left(1+\Gamma\right)}\right]^2\right]\frac{E_1}{11G_{13}}} \quad \text{with} \quad \Gamma = 1.18\frac{\sqrt{E_1 E_2}}{G_{13}} \tag{10}$$

The subsequent falling part of the load-displacement relationship is given by [8]:

$$\Delta_{\mathrm{I}} = \frac{2\left(wG_{\mathrm{I,c}} E_1 I\right)^{3/2}}{3E_1 I P^2} \tag{11}$$

The numerical responses for different specimen thicknesses are compared with the above analytical solutions in Fig. 9. It can be seen from the curves plotted that the finite element solutions are in very close agreement with the analytical predictions.

Some issues related with the numerical solution of the DCB problem are now considered. In Fig. 8a the finite element results for nominal thickness and average $G_{\mathrm{I,c}}$ have been compared with the experiments. The experimental results are found to be 1.6 times stiffer than this numerical response by simple inspection of the curves. One may argue that the difference in the elastic responses can be solved by adopting a "*corrected*" value of the modulus of elasticity $E_1^* = 1.6E_1 = 18400\,\mathrm{N/mm^2}$. Fig. 10 shows the improvements obtained by this modification to input data. It can be seen that the numerical elastic solution agrees well with the experiments and the damage propagation curves follow the same trend. The finite element results for this "*corrected*" are considered for further comparisons (FE_t=2.5_GI,c=1.8_1.6E1 in the graph in Fig. 10). The load versus crosshead displacement behaviour for this specific case is shown in Fig. 11. Three load levels are identified, corresponding to the onset of delamination, the maximum load and a load level corresponding to 80% of the maximum load on the descending portion of the curve. Some modelling results for the delamination development and growth in the DCB specimen are shown in Fig. 12 for these three load levels. The contour plots for the variable *Stiffness DEgradation Scalar* (SDEG) [1], which indicates the state of damage in the cohesive elements and thereby provides insight into the damage initiation and propagation, are shown. Complete interlaminar delamination is predicted when SDEG = 1. The deformed shape is also illustrated (magnification factor = 1). The contours show that the damage propagates from the initial flaw and that such propagation has a stable crack front.

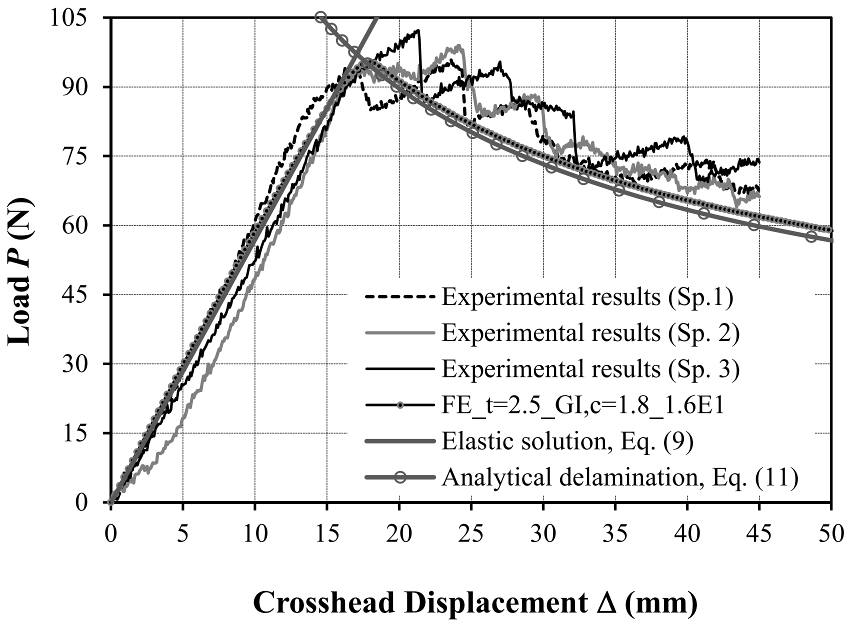

Fig. 10 Load versus crosshead displacement: comparison between experimental, analytical and numerical results using the "*corrected*" modulus of elasticity, the nominal thickness and the mean value of critical energy release rate

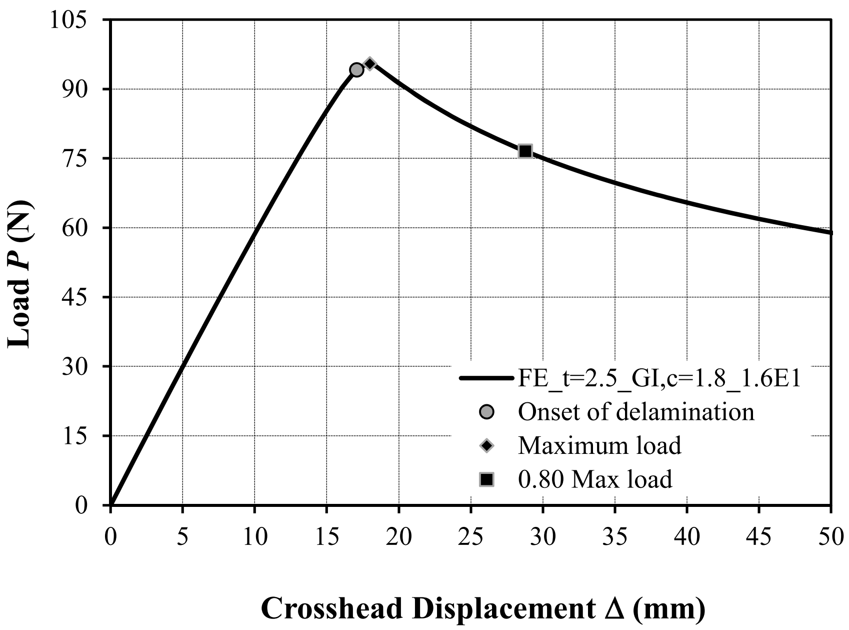

Fig. 11 Load versus crosshead displacement: numerical response using the "*corrected*" modulus of elasticity, the nominal thickness and the mean value of critical energy release rate

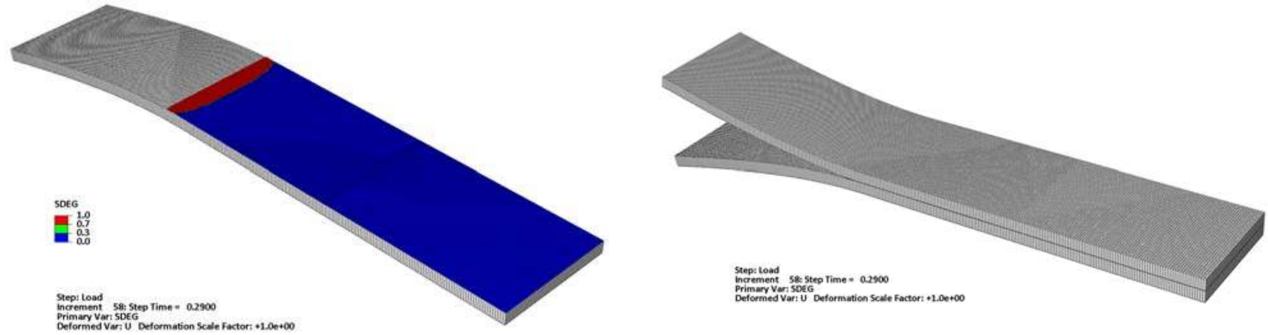

a) Onset of delamination: $P = 94$ N

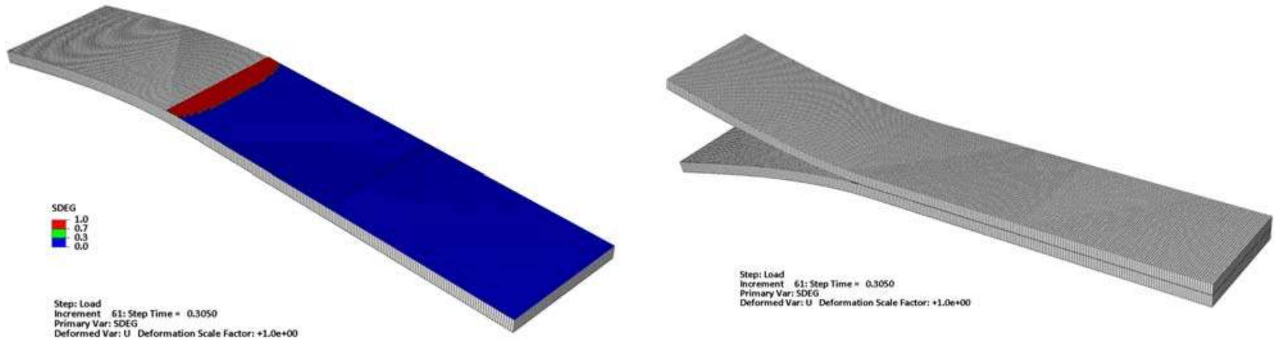

b) Maximum load: $P = 96$ N

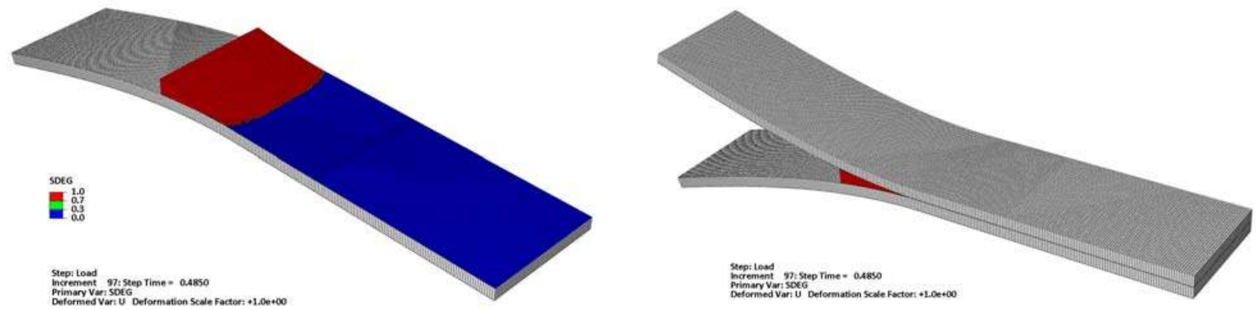

c) 0.80 of the maximum load: $P = 77$ N

Completely damaged Partially damaged Undamaged

Fig. 12 Evolution of mode I delamination zone in the DCB test specimen

3.1.2 Mode II Delamination

Mode II delamination fracture is caused by interlaminar shear that results in a sliding motion between two adjacent plies. To evaluate the pure mode II critical strain energy release rate, a three point bending apparatus is used to conduct an ENF test, as depicted in Fig. 13. Delamination fracture is constrained to grow between two unidirectional plies with their interface at mid-plane. The load is applied under displacement control and eventually a delamination crack initiates from the end of the pre-crack length a_0 and propagates to the midspan, and further in a very sudden way. The specimen geometry and boundary conditions, the carbon fibre laminate and interfacial properties for a mode II finite element analysis are as specified in Fig. 13 and Table 2. These are based on experimental and numerical data presented in ref. [13]. The initial crack length a_0 is 39.2 mm. A consistent element length of 0.5 mm was again used.

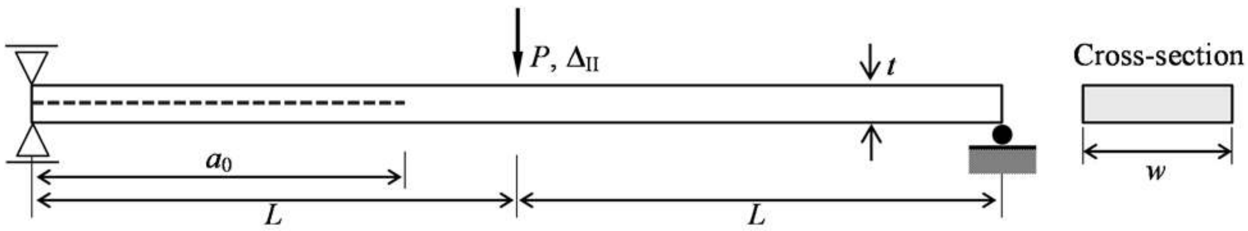

$2L = 102$ mm $\quad a_0 = 39.2$ mm $\quad t = 3.12$ mm $\quad w = 25.4$ mm

Fig. 13 ENF benchmark test coupon geometry

Table 2 Material properties of the ENF specimen

Lamina properties		Interfacial properties	
E_1 (N/mm^2)	122700	$G_{I,c}$ (N/mm)	0.97
$E_2 = E_3$ (N/mm^2)	10100	$G_{II,c} = G_{III,c}$ (N/mm)	1.72
$G_{12} = G_{13}$ (N/mm^2)	5500	f_I (N/mm^2)	80
G_{23} (N/mm^2)	3700	$f_{II} = f_{III}$ (N/mm^2)	100
ν_{12}	0.25	$K_I = K_{II} = K_{III}$ (N/mm^3)	10^6

The closed-form solutions for the load-carrying behaviour of the three point ENF specimen are obtained using the same principles as for the DCB specimen. Four curves define the load, P, versus deflection in the middle of the specimen, Δ_{II}:

$$\begin{aligned}
&\text{Analytical linear part} && \Delta_{II} = \frac{P\left(3a_0^3 + 2L^3\right)}{96E_1 I} \\
&\text{Analytical delamination } \left(a < L\right) && \Delta_{II} = \frac{P}{96E_1 I}\left[2L^3 + \frac{\left(64G_{II,c}wE_1 I\right)^{\frac{3}{2}}}{\sqrt{3}P^3}\right] \\
&\text{Analytical delamination } \left(a \geq L\right) && \Delta_{II} = \frac{P}{24E_1 I}\left[2L^3 - \frac{\left(64G_{II,c}wE_1 I\right)^{\frac{3}{2}}}{4\sqrt{3}P^3}\right] \\
&\text{Completely split beam} && \Delta_{II} = \frac{PL^3}{12E_1 I}
\end{aligned} \tag{12}$$

where L represents half-length of the beam and a is the crack length.

Fig. 14 plots the load P against the central deflection Δ_{II}. The numerical curve is characterized by an initial elastic behaviour associated with the initial crack length $a_0 = 39.2$ mm (segment OA) followed by a slight reduction in stiffness corresponding to damage initiation (segment AB) up to a peak load of 722 N is reached (point B). A softening region (segment BC) follows on, with a rapidly decreasing load that attains a minimum of 607 N at point C, and corresponds to the crack length front reaching the half length of the beam. A final re-hardening curve (segment CD) develops with the crack front advancing further until the beam is completely split. There is a close agreement between the finite element results and the analytical solutions by Eqs. (12). However, the experimental results are in poor agreement with both finite element and analytical solutions for post-delamination initiation. Fig. 15 refers to the finite element results for mode II delamination fracture and identifies four load levels corresponding to (i) the onset of delamination, which is the elastic limit load in this specific case, (ii) minimum load in the softening branch that corresponds to 84% of the elastic limit load, (iii) same value of the elastic limit load in the ascending branch, and (iv) 120% of the previous load level.

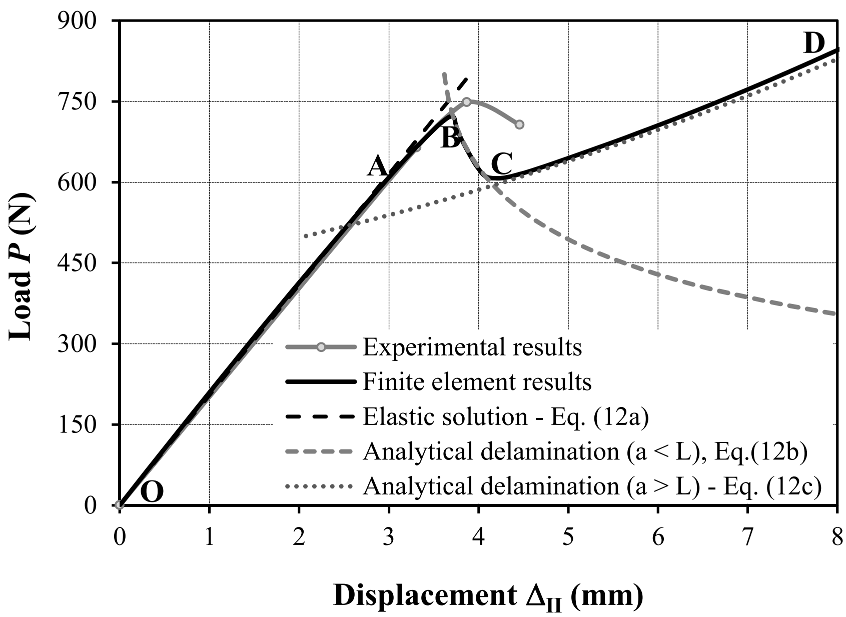

Fig. 14 Load versus central displacement: comparison of results

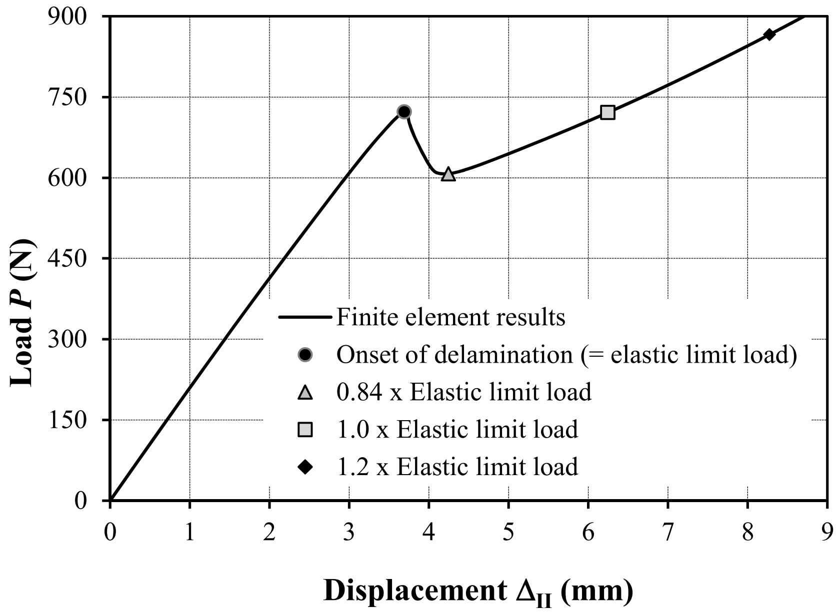

Fig. 15 Load versus central displacement: finite element results

In Fig. 16 the delamination zone of the plate and the specimen deformed shape are shown at several load levels during the computation (see Fig. 15). The delamination damage (variable SDEG) grows uniformly with the load. The deformed shape clearly shows the relative sliding between the two sub-laminates as expected for the pure mode II delamination failure.

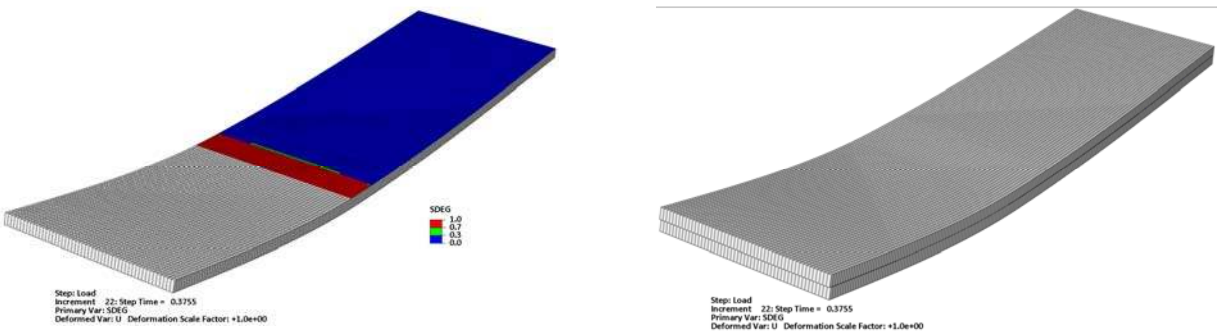

a) Onset of delamination: $P = 720$ N

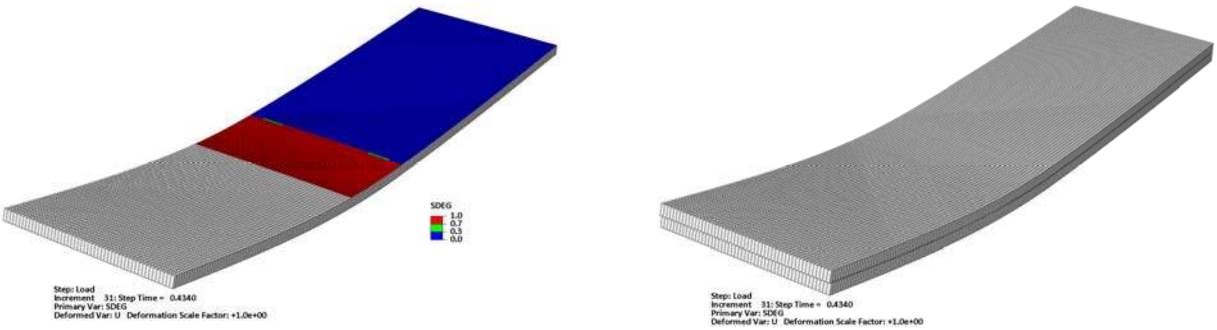

b) Minimum load past post-initiation of delamination: $P = 605$ N

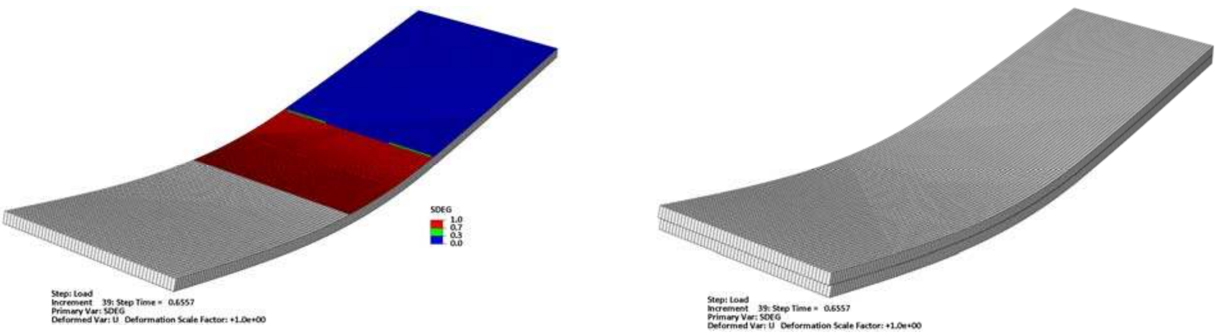

c) Load level equal to the elastic limit load past post-initiation of delamination: $P = 720$ N

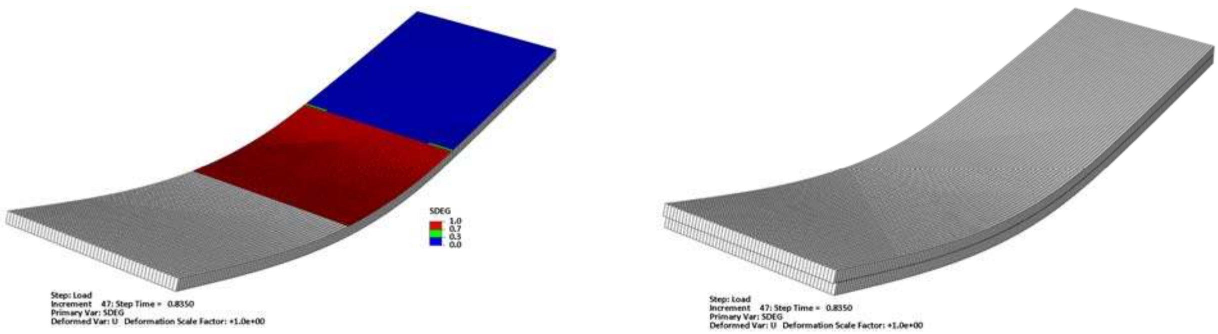

d) 1.20 of the elastic limit load past post-initiation of delamination: $P = 720$ N

Completely damaged Partially damaged Undamaged

Fig. 16 Evolution of mode II delamination zone in the ENF test specimen

3.2 Notched Laminates under In-Plane Tensile Loading

In-plane failure of composites may be governed by two possibilities:

- Delamination and matrix cracking that coalesce to produce a fracture surface.
- Fracture of the fibres.

Whilst the second failure mode is a quasi-brittle fracture type, the first is expected to possess damage tolerance and is especially important at stress concentrations such as notches. Both failure events are analysed in this section.

The numerical studies presented in this section include a continuum damage model with a cohesive zone approach to composite modelling. Continuum damage models address the intralaminar failure mechanisms from a global view, where individual damage mechanisms are homogenized and constructed around a failure criterion. This approach is the least complex and uses the composite layup modeller tool within the Abaqus pre-processor to define the individual ply layers through the laminate thickness, each layer then being cohesively bonded together to form the laminate ply stack. Interface layers are assumed to have a thickness of $10^{-3}t_{\text{ply}}$, being t_{ply} the thickness of the ply. This dimension plays the role of a length scale and it will be shown that the thickness of the cohesive layer does not affect the model performance provided its value is small enough as compared to the ply thickness.

3.2.1 Laminate of Carbon/Epoxy with a Centre Crack

Here the static analysis of the delamination dominated progressive failure process in central-sharp notched carbon/epoxy laminates is examined and the predictions are compared with experimental and numerical results taken from the literature. This kind of analysis is relevant to assess the efficiency of a modelling strategy. In particular, perhaps the simplest (yet extremely important) composite layup is considered: a cross-ply laminate with a $[90/0]_s$ arrangement.

The dominant failure mechanisms in cross-ply laminates subjected to mechanical loading are (i) transverse matrix cracking in the 90° plies around the notch, (ii) splitting, i.e. longitudinal matrix cracking that propagates from the notch along the direction of the 0° plies, and (iii) delamination between the 0° and 90° plies, which consist of narrow regions elongated along the load direction and developing transversely from the splitting. The laminate tensile strength is usually reached as a result of excessive delamination. In some cases, specimens can fail by fibre breakage rather than by gross delamination. The role of delamination in fibre-dominated failure notched specimens is analysed in Section 3.2.2. The governing failure mode naturally depends on the relative delamination and fibre failure stresses.

Initial Results The specimen is modelled with one-quarter symmetry finite element mesh, as shown in Fig. 17 for the particular case of the laminate with a centre sharp crack tested experimentally by Spearing and Beaumont [73], and numerically by Wisnom and Chang [74] and van der Meer *et al*. [75]. (The two numerical approaches to the matrix-crack failure processes are different, as explained above.) The model is built up from stacked continuum shell elements, with each individual ply being modelled as a separate layer. Cohesive interface elements connect the two plies to allow for delamination damage. The in-plane mesh of the interface is the same as that of the ply. A monotonic longitudinal tensile load is applied in the form of an applied uniform displacement δ in the direction of the longitudinal axis at both ends. The analysis is performed using a global stabilization factor of 2×10^{-4}.

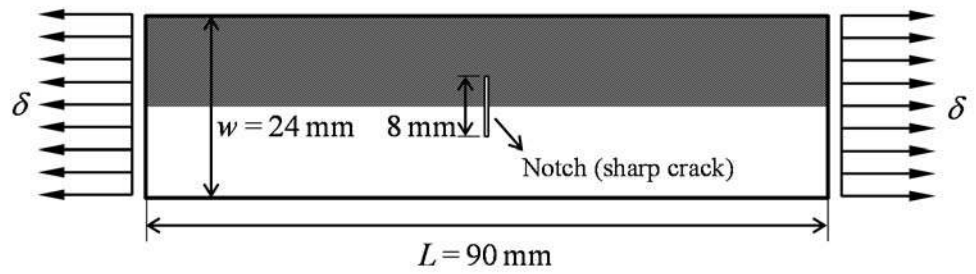

a) Schematic

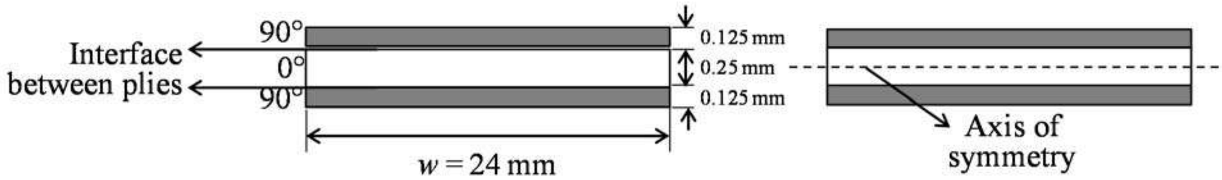

b) Layup

Fig. 17 Specimen geometry (Spearing and Beaumont [73])

The continuum material model adopted in the commercial finite element code Abaqus for the analysis of progressive intralaminar failure (Section 2.2) is used in the numerical simulations. Early work on the progressive modelling of the splitting crack that grows from the notch tip in the 0° ply and the transverse cracks in the 90° ply used spring or interface elements [52,74,76,77]. This requires the specification of the crack in advance. More recently, van der Meer and Sluys [78] showed that this failure mode could be similarly captured by using continuum models that do not require any assumption on the crack localization and thus show a better predictive potential. Failure in the interface elements is modelled with the damage law presented in Section 2.3. The material properties used in the current analysis are summarized in Table 3. Most parameters in the table are taken from refs. [73,74]. The lamina strength properties in compression and shear are taken from Hancox and Mayer [79]. The interfacial strength properties were reduced from those of the matrix by adopting a weakening factor f_w, according to Puck's guidelines [27,28]. It was found that the overall response for $f_w = 0.5$ is the one closer to the experimental results, which may indicate a weaker interface. Other values for f_w are also analysed below to provide insight on the effects of the chosen values on the strength behaviour of this specific notched laminate. The fracture energy related to fibre breakage is assumed to be 100 N/mm, in line with the values proposed by Pinho *et al*. [80].

Table 3 Lamina and interfacial properties of the laminate with a centre crack

Elastic lamina properties		Lamina strength properties		Fracture energy		Interfacial properties	
E_1 (N/mm^2)	135000	$f_{1,T}$ (N/mm^2)	1673	$G_{1,T,c}$ (N/mm)	100	$G_{I,c}$ (N/mm)	0.15
$E_2 = E_3$ (N/mm^2)	9600	$f_{1,C}$ (N/mm^2)	1500	$G_{1,C,c}$ (N/mm)	100	$G_{II,c} = G_{III,c}$ (N/mm)	0.4
$G_{12} = G_{13}$ (N/mm^2)	5800	$f_{2,T}$ (N/mm^2)	60	$G_{2,T,c}$ (N/mm)	0.15	f_I (N/mm^2)	30
G_{23} (N/mm^2)	4000	$f_{2,C}$ (N/mm^2)	150	$G_{2,C,c}$ (N/mm)	1.1	$f_{II} = f_{III}$ (N/mm^2)	37.5
ν_{12}	0.31	$f_{1,S} = f_{2,S}$ (N/mm^2)	75			$K_I = K_{II} = K_{III}$ (N/mm^3)	3×10^5

The finite element mesh used in our study has a total of 63056 continuum shell SC8R elements, and 31258 COH3D8 cohesive elements, and is shown in Fig. 18. A preliminary analysis is run with the nonlinear material properties from Table 3 assigned to the plies. Although this is the most realistic numerical model, the actual failure behaviour cannot be captured. The damage observed experimentally consisted of transverse matrix cracking, delamination and longitudinal splitting [73]. The proposed finite element model initiates and propagates the split in the 0° ply, as shown in Fig. 19a. Following this split, a band of localized matrix failure appears in the 90°ply, as can be seen in Fig. 19b. Because this process requires less energy, delamination between plies does not occur, see Fig. 19c. This is an unrealistic failure mode that has already been observed in numerical simulations by van der Meer and Sluys [77]. In order to allow delamination between plies to occur, a second analysis is performed under the assumption of linear behaviour in the outer 90° ply. This approach does not cater for the representation of transverse matrix cracks in the off-axis ply. Nevertheless, this mode of failure is not significant for the overall behaviour when compared to the splitting and delamination modes, as shown by van der Meer [81]. In Fig. 20 the final deformed mesh is shown.

The longitudinal split that develops at the 0° ply (top ply in the figure) can be clearly observed, as well as the shear mode delamination (sliding and tearing modes), see Figs. 20a and 20b, respectively. The tensile stress (i.e. the applied load averaged over the nominal gross cross-section) versus the end displacement plots for the current modelling approach are compared with the finite element predictions from van der Meer [81] in Fig. 21. Results are in good agreement, not unexpectedly as both represent acceptable formulations of the problem, and this provides validation for the Abaqus model used here.

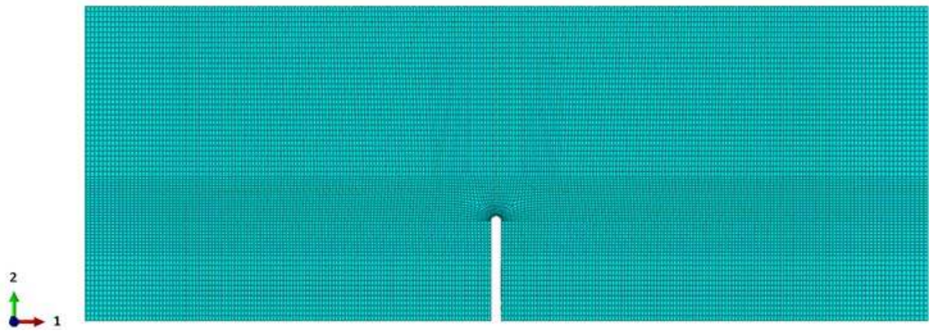

Fig. 18 Mesh of the model implemented for the analysis of the laminate with a centre crack

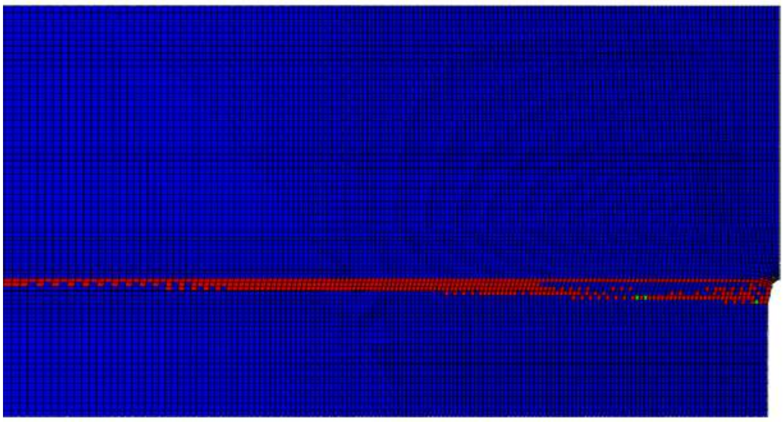

a) 0° ply

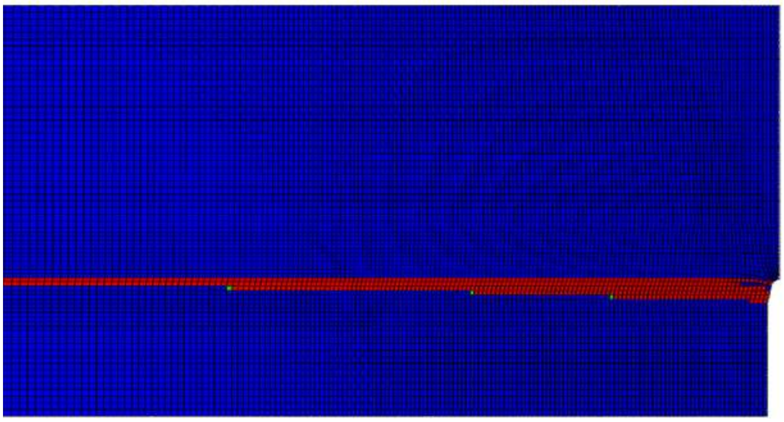

b) 90° ply

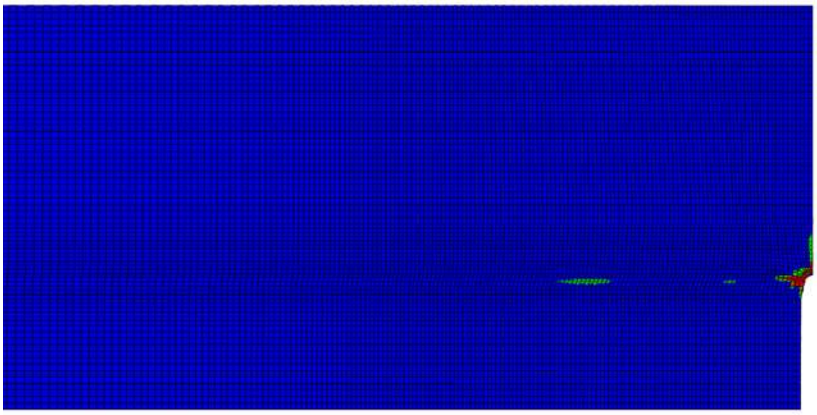

c) Interface (incipient delamination)

Completely damaged Partially damaged Undamaged

Fig. 19 Damage plot of ultimate failure mechanisms (tensile strength 275 MPa) for both plies with continuum damage

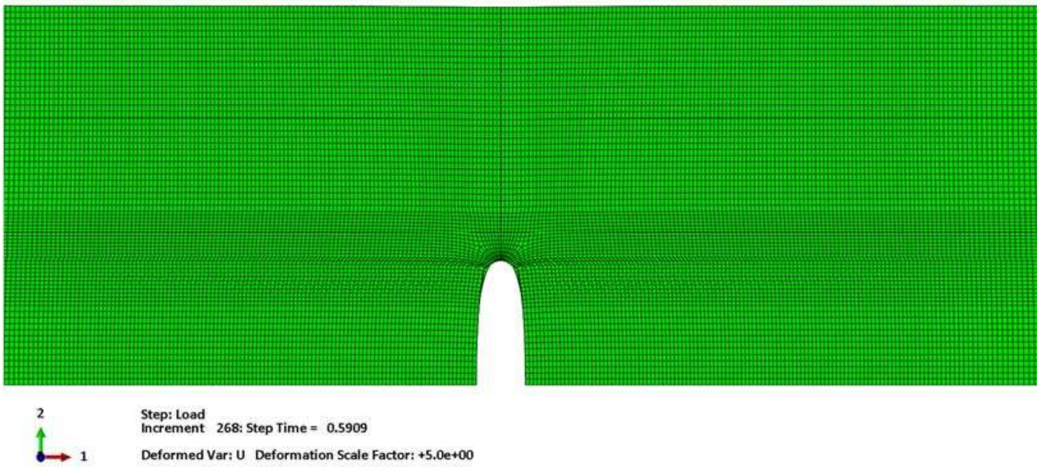

a) In-plane view

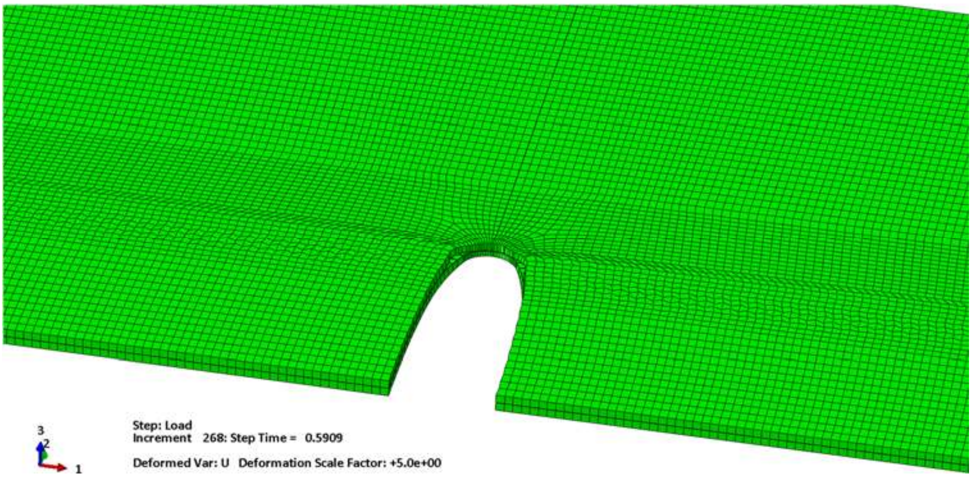

b) Detail of the deformation of the two plies near the centre crack

Fig. 20 Final deformed mesh from analysis with continuum damage 0° ply and elastic 90° ply (magnification factor of 5)

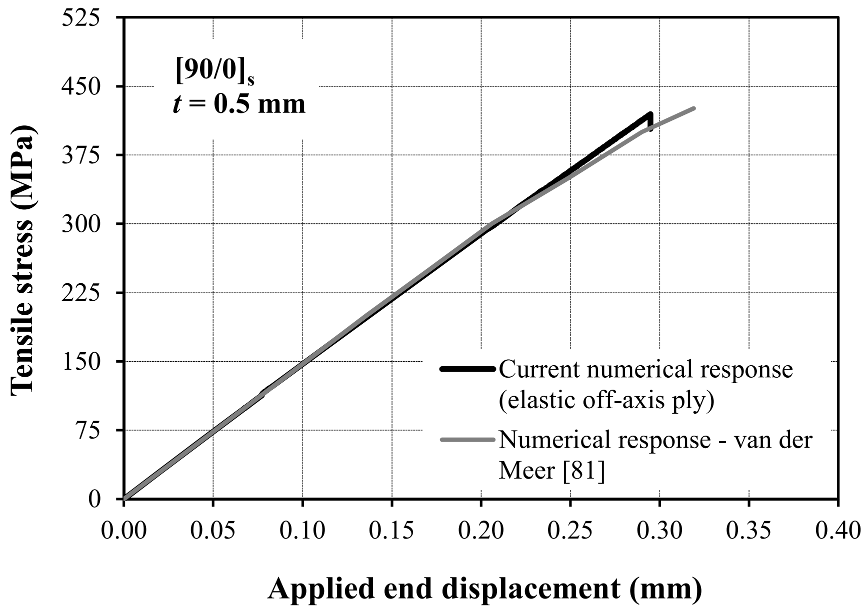

Fig. 21 Tensile stress-end displacement plot resulting from implementing the finite element model with continuum damage 0° ply and elastic 90° ply, and comparison with existing numerical data

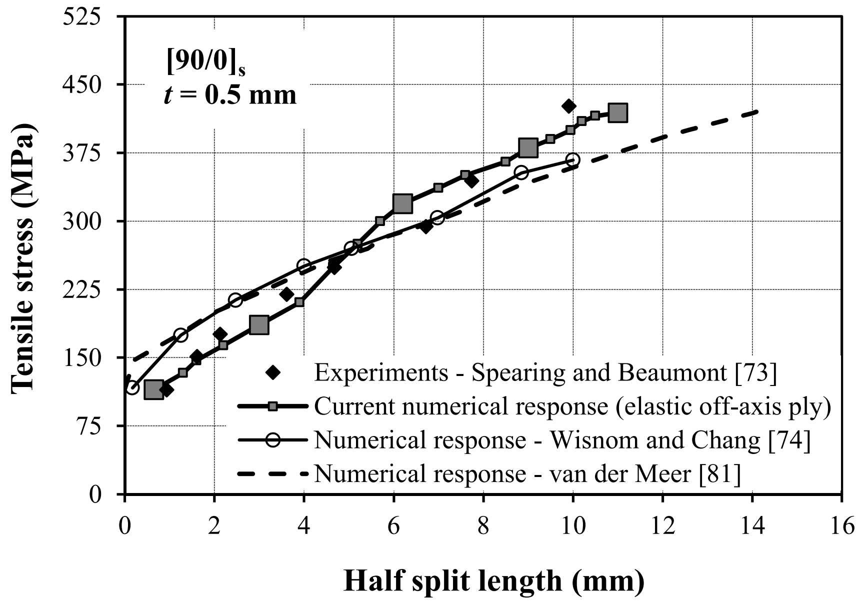

Fig. 22 Tensile stress-half split length plot resulting from implementing the finite element model with continuum damage 0° ply and elastic 90° ply, and correlation to predicted and measured splitting

Fig. 22 shows the (half) split length, L_{split}, i.e. the length of the discontinuity in the 0° ply which originates and propagates from the notch tip to each end, as a function of the tensile stress applied to the specimen. Our results are compared with the experimental observations of Spearing and Beaumont [73] and the numerical predictions from Wisnom and Chang [74] and van der Meer [81]. Current predictions show a better agreement with the experiments. The current finite element model underestimates the strength by 1.5% and overestimates the half split length by 11%. Finally, Fig. 23 gives split and delamination plots at incipient interlaminar failure and subsequent propagation for the specific stress levels and corresponding half split lengths displayed in Fig. 22 as large squares. The growth of delamination between the two plies is stable. The width and length of the delamination area is 0.65 mm and 11 mm, respectively, when the laminate strength is reached. This gives a predicted angle of 3.4° that compares very well to the experimentally observed angle of the delamination front of 3.5°. The delamination extent is consistently less than the split length and this is also in line with the numerical results from Wisnom and Chang [74]. The pattern of delamination can be roughly approximated by a triangular shape, as seen in the tests of Spearing and Beaumont [73].

The current finite element simulations are able to mimic the most significant failure modes that are observed in the experiments and other numerical works. Comparisons with reported stress-displacement and stress-half split length validate the global behaviour predicted by the proposed model. Further comparisons with damage patterns confirm the accuracy of our approach for the modelling of matrix cracking and delamination. The model is not validated for fibre breakage as this was not a governing failure mode in the notched laminate analysed.

The notch strength reduction factor *k*, defined as the ratio between the actual notched laminate strength and the unnotched strength, is 0.5 for this specific example, which suggests that a centre crack with half of the laminate width has a detrimental effect in the overall resistance.

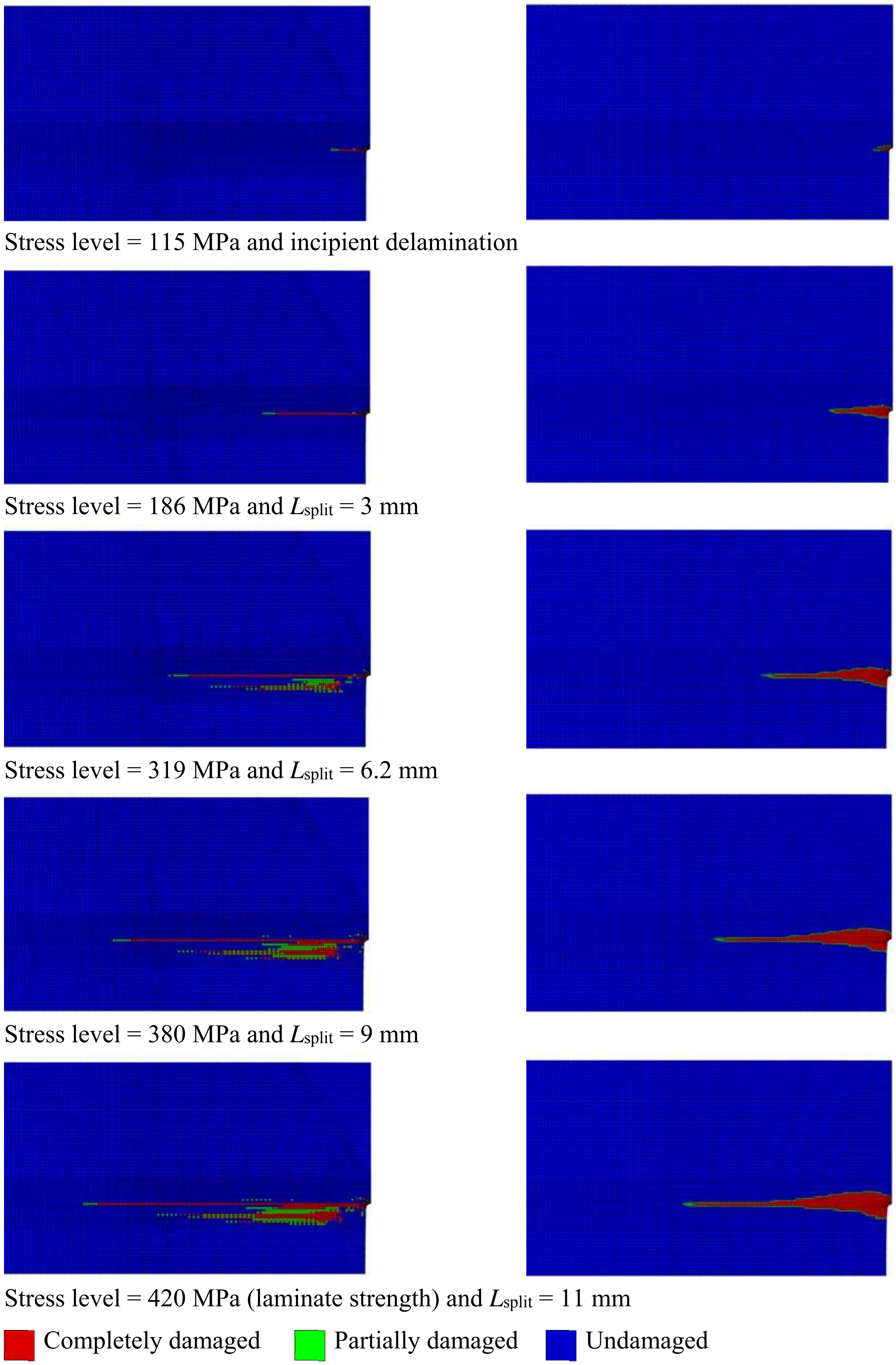

a) 0° ply **b)** Interface

Fig. 23 Split and delamination onset and propagation with applied load the damage in the 0° ply and in the interface at maximum (numerical) tensile strength.

Numerical Interfacial Strength Sensitivity Study Simulations are now carried out for different weakening factors for the interface strength (or interfacial strength values) while keeping the critical energy release rate constant in order to develop an understanding of the interfacial effect on failure of notched composites. The following values of f_w are selected to be 1.0 (perfect interface), 0.85 (strong interface), 0.35 and 0.25 (weak interface). The corresponding half split length and laminate strength, σ_{max}, are shown in Table 4. The strength ratios to the baseline model ($\sigma_{max,base}$ for f_w = 0.5) are also computed. The stress level at incipient delamination, σ_{del}, is given as a ratio to the laminate strength. It is interesting to find that the laminate strength is very much dependent on the value of the interfacial strength. It is also found that the laminate strength does not vary proportionately to that of the interface. In terms of numerical analysis, this implies that there is an optimum value for this property as far as longitudinal tensile test is concerned. A very strong interface may result in a brittle failure of the composite thereby decreasing the strength (in about 20% for this specific case). It is worthwhile to note that in this case there is hardly any variation in the half split length. Similar results are observed for very weak interfaces, for which delamination starts at lower stress levels. In these cases, and as expected, the split length increases. These are important points to be considered while selecting specific interfacial strength values for a given problem.

Table 4 Effect of interfacial strength

Model	f_w	L_{split} (mm)	σ_{max} (MPa)	$\sigma_{max}/\sigma_{max,base}$	$\sigma_{del}/\sigma_{max}$
Baseline	0.5	11.0	420	1.0	0.27
A	1.0	11.2	327	0.78	0.30
B	0.85	11.3	343	0.82	0.29
C	0.35	15.0	388	0.92	0.26
D	0.25	16.5	340	0.81	0.22

3.2.2 Double-Edge-V-Notched Laminate

This data set is taken from the experimental work conducted by Hallett and Wisnom [82] for E-glass/epoxy double-edge-notched cross-ply laminates. Fig. 24 shows the notched plate geometry and Table 5 sets out the material properties. The half of the geometry shaded in the plane view is modelled.

Experiments at Bristol University show that ultimate failure is governed by fibre breakage in the 0° ply. Failure of the fibres starts at the notch tip and propagates across the laminate width and is preceded by longitudinal splitting and delamination. The laminate eventually fails in a brittle way, with a crack running perpendicular to the fibre direction. Initiation and progression of failure in this case occurs through several competing and interacting mechanisms. The computational modelling now has to account for these three failure mode interactions.

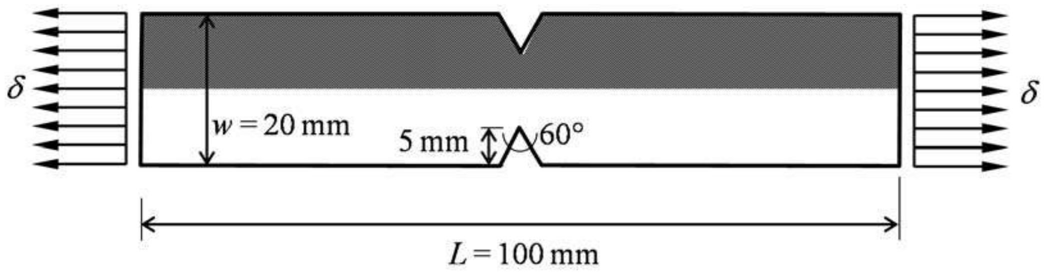

a) Schematic

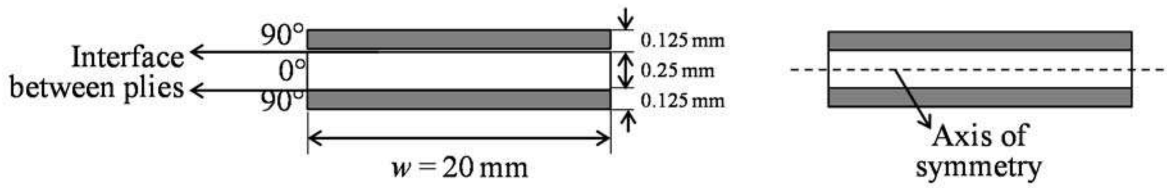

b) Layup

Fig. 24 Specimen geometry (Hallett and Wisnom [82])

Table 5 Lamina and interfacial properties of the double-edge-notched laminate

Elastic lamina properties		Lamina strength properties		Fracture energy		Interfacial properties	
E_1 (N/mm^2)	43900	$f_{1,\mathrm{T}}$ (N/mm^2)	1060	$G_{1,\mathrm{T,c}}$ (N/mm)	80	$G_{\mathrm{I,c}}$ (N/mm)	0.25
$E_2 = E_3$ (N/mm^2)	15400	$f_{1,\mathrm{C}}$ (N/mm^2)	2000	$G_{1,\mathrm{C,c}}$ (N/mm)	100	$G_{\mathrm{II,c}} = G_{\mathrm{III,c}}$ (N/mm)	1.8
$G_{12} = G_{13}$ (N/mm^2)	4340	$f_{2,\mathrm{T}}$ (N/mm^2)	75	$G_{2,\mathrm{T,c}}$ (N/mm)	0.25	f_{I} (N/mm^2)	56
G_{23} (N/mm^2)	4340	$f_{2,\mathrm{C}}$ (N/mm^2)	120	$G_{2,\mathrm{C,c}}$ (N/mm)	0.75	$f_{\mathrm{II}} = f_{\mathrm{III}}$ (N/mm^2)	75
ν_{12}	3200	$f_{1,\mathrm{S}} = f_{2,\mathrm{S}}$ (N/mm^2)	88			$K_{\mathrm{I}} = K_{\mathrm{II}} = K_{\mathrm{III}}$ (N/mm^3)	1×10^6

A preliminary model based on a continuum damage approach for individual plies (as above, the off-axis ply behaves elastically) and a cohesive zone model for the interface is developed. The finite element mesh density used in the current study is identical to the above model. In order to trigger fibre fracture, the fracture energy related to fibre failure is reduced by 90% of its original value (see Table 5) in a 0.25 mm wide localization band at the net-tension plane [83]. This band is wider than the finite elements to ensure the mesh objectivity of the results. In this model, the element sizes in the notch area are about 0.125 mm.

Figs. 25 and 26 show the global stress-strain response under the applied tensile load and the damage in the 0° ply and in the interface at maximum (numerical) tensile strength. The following observations can be made:

1. The numerical response is linear until a maximum (tensile strength) is reached at which a load drop is observed. The tensile strength is 174 MPa. This number does not compare well against the measured experimental strength (267 MPa) reported by Hallett and Wisnom [82].
2. The interaction of matrix failure, in the form of splitting and delamination, and fibre failure does not agree qualitatively with the experimental observations.
3. The failure patterns show (i) a band with fibre-tension damage (Fig. 26a), which determines the laminate strength, (ii) longitudinal splitting crack that grows from the notch tip (Fig. 26b), and also matrix cracking damage smeared out over the elements, with rows of damaged elements opposite the notch tip.
4. Although the interface between the two plies delaminates (Fig. 26c), the extent of delamination damage is much less severe than that observed in the experiments.

Clearly, the numerical model is not able to capture both global and local behaviours. The fact that the matrix cracking is too smeared out over the elements, rather than being a discrete crack, does not allow the notch to blunt and delay the onset of fibre failure. As a consequence, the predicted tensile strength is very low as compared to the measured value.

In order to solve this problem, the finite element model was reformulated to enable the individual representation of the damage modes. The matrix longitudinal splitting in the 0° ply is now forced to localize and is modelled as a strip tangent to the notch. This method is very similar to the localization band approach to fibre-tension damage simulation and is a relatively simple approach to circumvent some of the limitations of the continuum damage models when the fracture path is known *a priori*. Although the continuum description of laminate failure is still present, this method implies the specification of the location of splitting in advance as matrix damage is confined to the pre-defined strip. This strip is 0.22 mm wide in this problem (again, wider than the typical element size) and is assigned with the mechanical properties summarized in Table 5. The rest of the laminate behaves elastically.

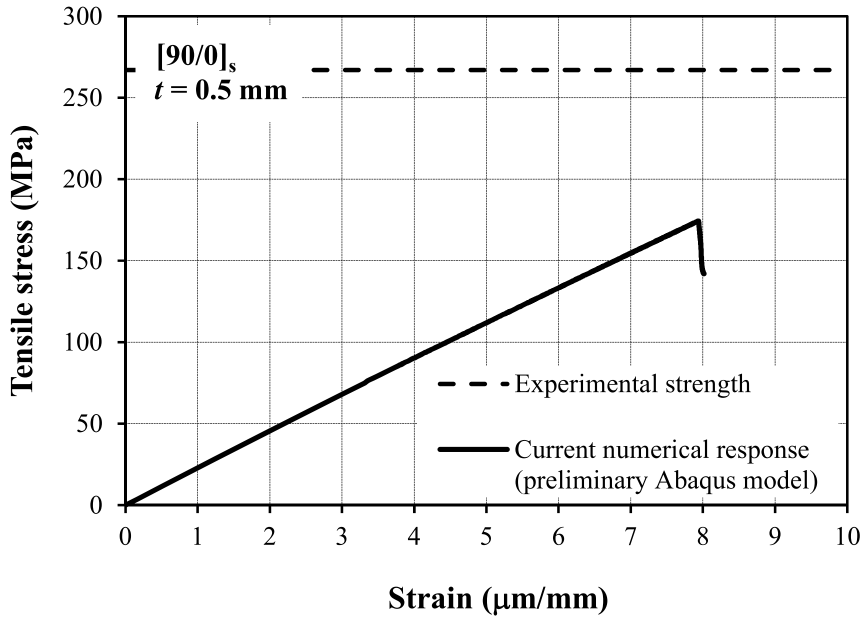

Fig. 25 Tensile stress-strain plot resulting from implementing the preliminary finite element model with continuum damage 0° ply and elastic 90° ply, and comparison with existing experimental data

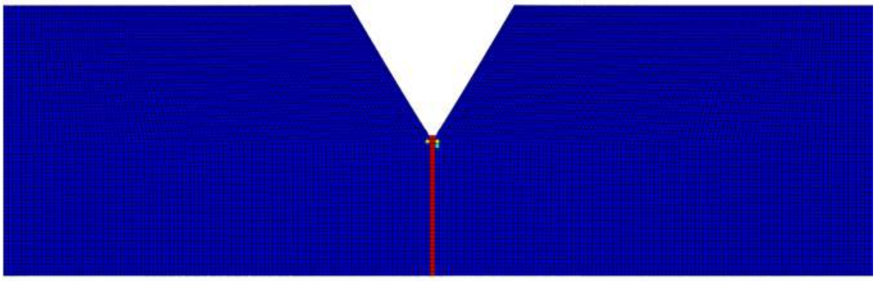

a) 0° ply: fibre-tension damage

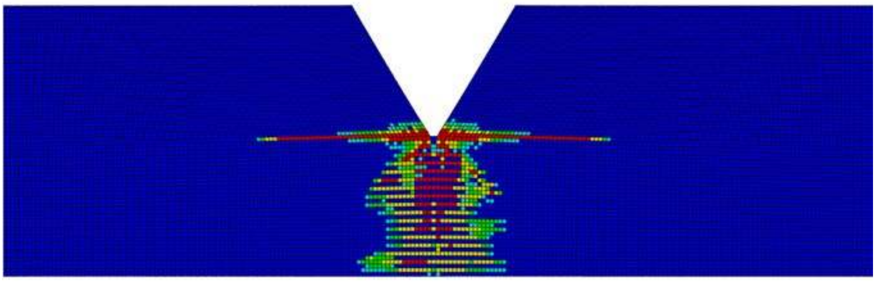

b) 0° ply: longitudinal splitting

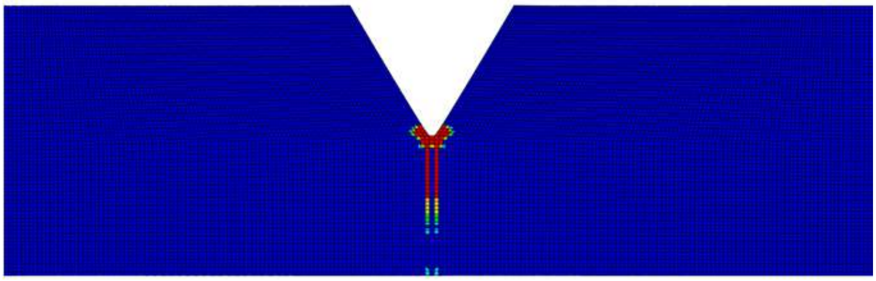

c) Interface: delamination

Completely damaged Partially damaged Undamaged

Fig. 26 Damage plot of ultimate failure mechanisms (tensile strength 174 MPa) for 0° ply with continuum damage and interface

The model is now able to reproduce the correct sequence of failure events (see Fig. 27): (i) 0° splits emanating from the notch tip at about 30% of the failure load, (ii) 90°/0° ply-interface delaminations (at about 50% of the failure load) and increase in length of the splits, and (iii) fibre-tension fracture. Fig. 28 illustrates how the model also captures the correct deformation: (i) ply separation mainly caused by interlaminar shearing stresses, and (ii) blunting of the notch.

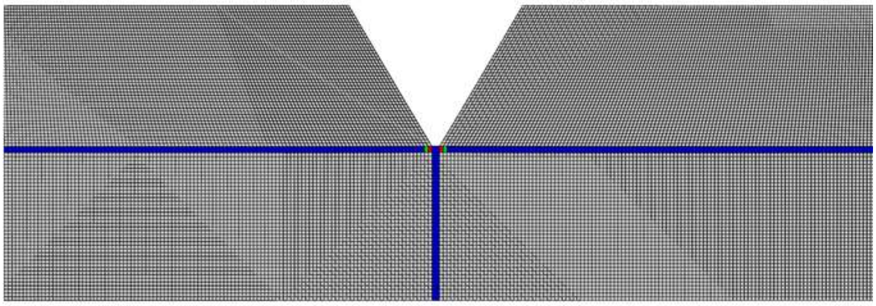

a) Damage initiation: longitudinal splitting ($\sigma = 80$ MPa)

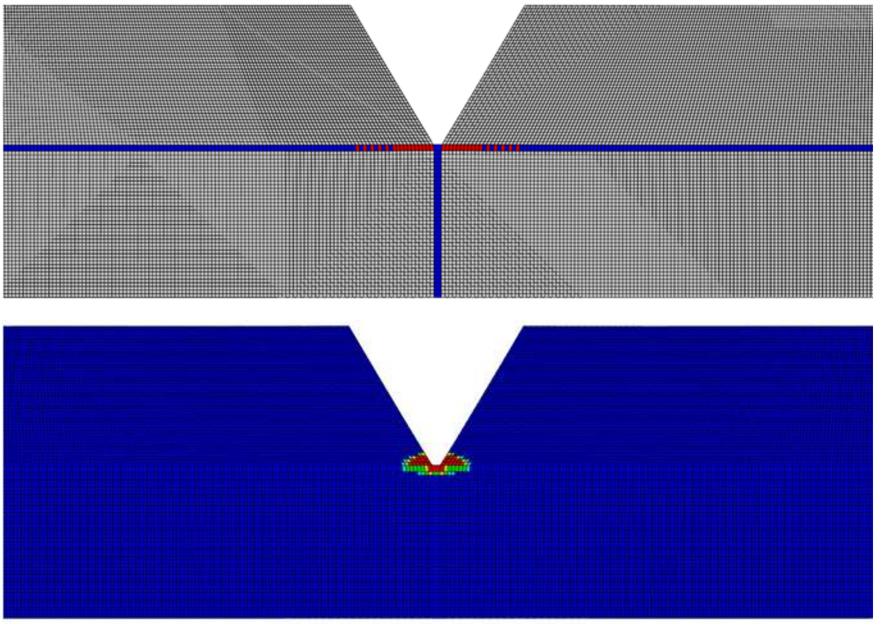

b) Damage progression: axial splits grow in length along the load direction and delaminations develop at the interface between the 90° and the 0° layers ($\sigma = 125$ MPa)

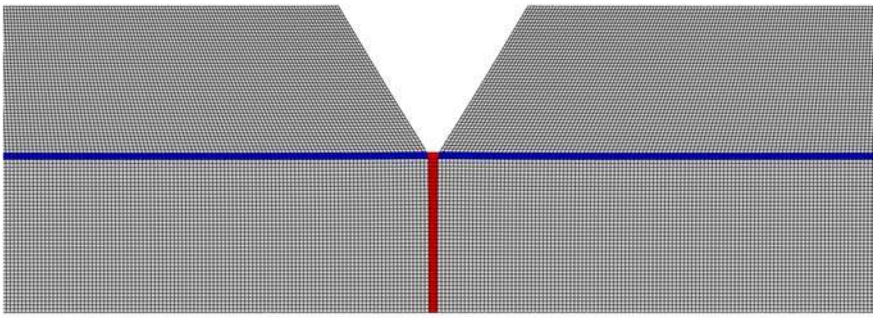

c) Fibre-tension fracture and final failure ($\sigma = 255$ MPa)

Completely damaged Partially damaged Undamaged

Fig. 27 Progressive damage from analysis with continuum damage 0° ply and elastic 90° ply, and localized longitudinal cracking in the 0° ply

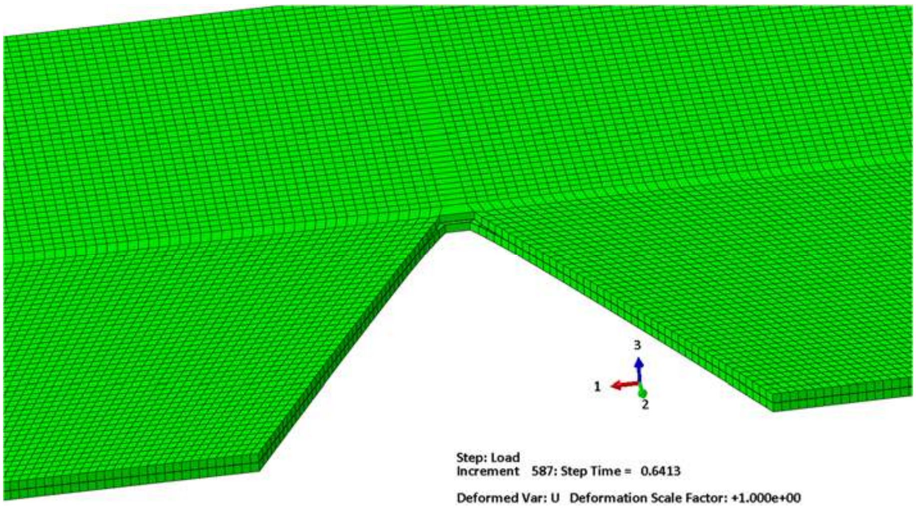

Fig. 28 Final deformed mesh from analysis with continuum damage 0° ply and elastic 90° ply, and localized longitudinal cracking in the 0° ply

Figs. 29 and 30 plot the current finite element predictions of tensile strength versus strain and half split length, respectively, and compare those predictions with the experimental data [82]. The experimental results and model predictions show good correlation both in terms of overall trend and the absolute values, despite the simplifications in the idealized model.

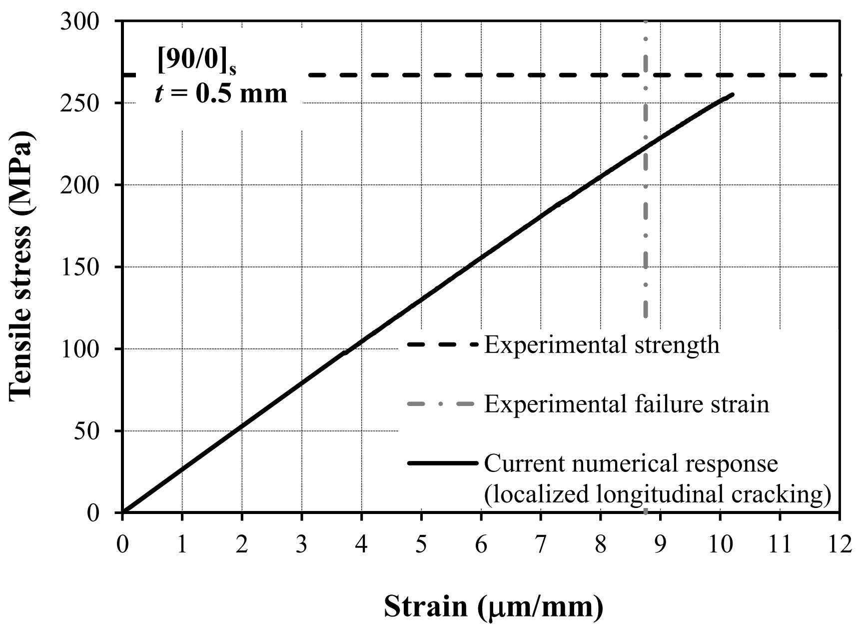

Fig. 29 Tensile stress-strain plot resulting from implementing the finite element model with continuum damage 0° ply and elastic 90° ply, and localized longitudinal cracking in the 0° ply; comparison with existing experimental data

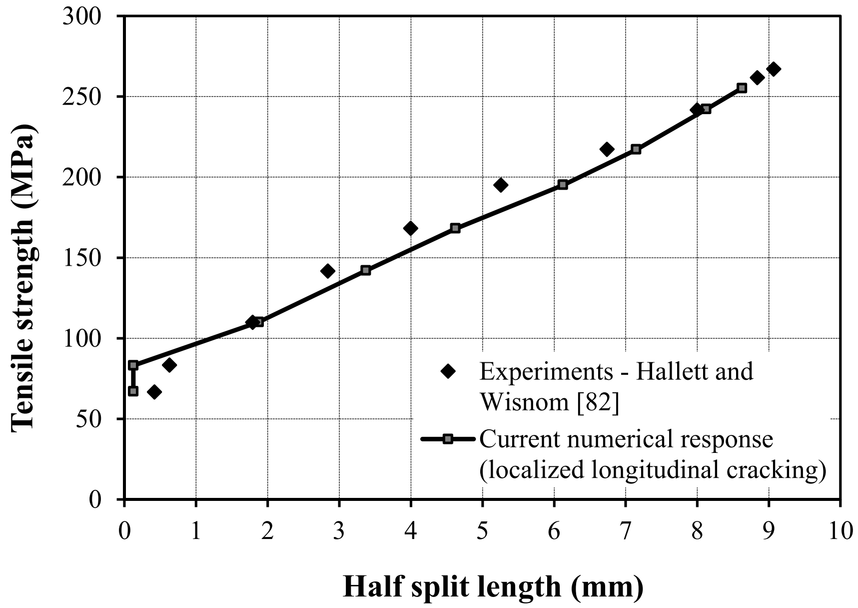

Fig. 30 Tensile stress-half split length plot resulting from implementing the finite element model with continuum damage 0° ply and elastic 90° ply, and localized longitudinal cracking in the 0° ply; correlation to measured splitting

Contours of the calculated intralaminar damage indices at an applied pull-plate stress of 200 MPa, equal to 78% of the ultimate strength are shown in Fig. 31. These contours have to be compared with identical numerical predictions by Hallett and Wisnom [82]. The agreement is, again, good, although the delamination patterns are slightly different. Our delaminations consist of narrow regions elongated along the load direction and developing transversally from the splitting, with a geometry slightly different from the triangular shape reported by Hallett and Wisnom [76,82]. Our pattern shows that the delamination at the interface also progresses to the centre of the laminate and to the free edge, see Fig. 32, as eventually happens when (ultimate) failure by the fibres occurs.

Overall, the current predictions for the V-notched specimen are fairly repeatable and accurate with respect to the experimental and numerical observations from Hallett and Wisnom [76,82]. This demonstrates the ability of our model to accurately predict failures in cases where the interaction between intralaminar and interlaminar modes is strongly coupled.

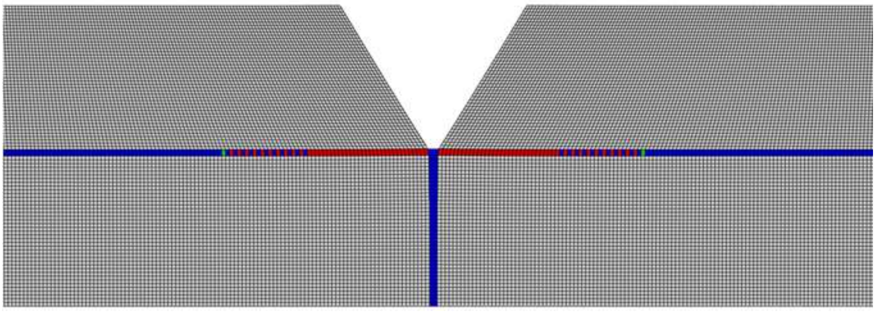

a) Longitudinal splitting

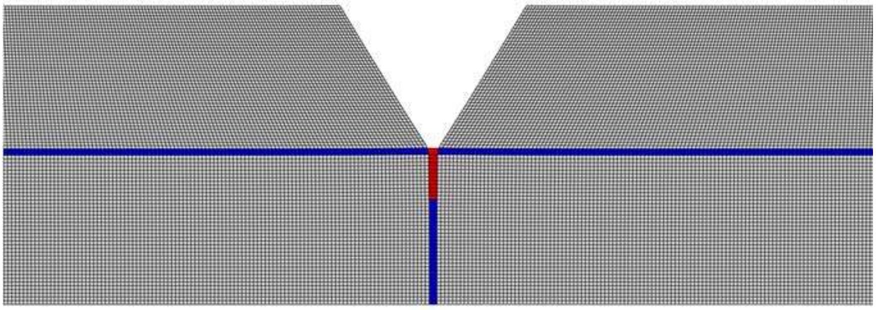

b) Fibre fracture

Completely damaged Partially damaged Undamaged

Fig. 31 Predicted damage at a stress level of 200 MPa from analysis with continuum damage 0° ply and elastic 90° ply, and localized longitudinal cracking in the 0° ply

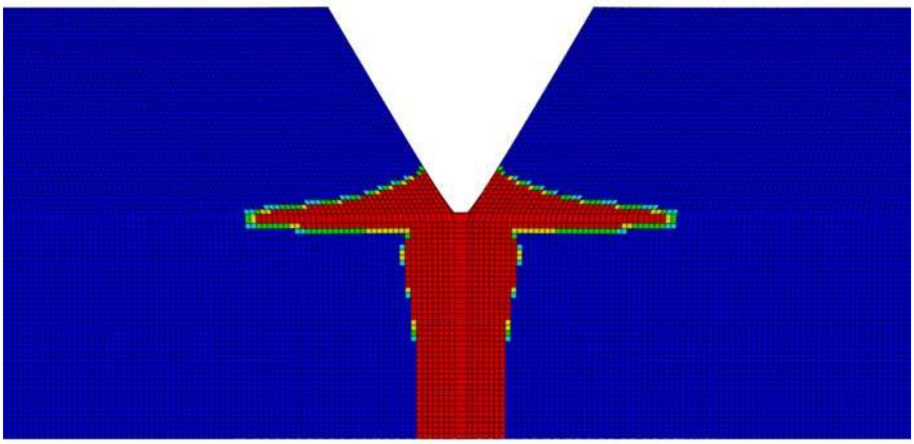

Completely damaged Partially damaged Undamaged

Fig. 32 Delamination pattern at final failure of the laminate

4 Summary of Modelling Guidance

In this study, a progressive damage approach for composite materials has been adopted using only the predictive capabilities of the general purpose software Abaqus. This results from a combination of the prediction of intralaminar damage initiation by means of the Hashin failure theory and a material damage model to simulate loss in the load-carrying capability of the part and advances the progression of damage based on mode-specific strain energy release rates. Similarly, a strength-based failure criterion adequately predicted the interlaminar failure which caused initial delamination onset. Delamination was predicted to extend by using the strain energy release rate analysis. The following guidelines are provided to address common problems faced by analysts when simulating the behaviour of cross-ply notched laminates under in-plane tensile loading:

1. Interface layers should not be thicker than $10^{-3}t_{\text{ply}}$.
2. Boundary conditions consistent with the geometric symmetry of the plates can and should be employed but not on the longitudinal direction as the conditions restraining movement may change the stress field.
3. Loads should be applied by imposing incremental displacements, as opposed to the classical load control method.
4. Global stabilization and artificial viscosity prevent numerical instabilities. The values proposed in this study are 2×10^{-4} and 1×10^{-5}, for the two coefficients (respectively).
5. In order to allow delamination to occur between plies in cross-ply laminates, the assumption of linear behaviour in the off-axis
6. By using implicit methods, the mesh density that ensured convergence to the "actual" results implies a minimum element size equal to the ply thickness around the notch, corresponding to the element sizes adopted in our models (see Section 3.2).
7. The split and fibre-tension localization bands width should be at least 1.25 times wider than the surrounding elements in the mesh.

5 Concluding Remarks

Computational structural modelling has been used to analyse delamination dominated failures in composite materials that were observed in physical and numerical tests of notched laminates of carbon/epoxy and E-glass/epoxy. It is shown that the proposed finite element approach is able to represent all the main features of the structural behaviour. In particular, it offers a reliable alternative to physical testing and to complex modelling that often relies on proprietary user-subroutines to define the material mechanical behaviour.

The study has highlighted the crucial role of delamination for in-plane failure by example of cross-ply notched laminates from the literature, where a characteristic pattern of damage initiating from the notch and propagating towards the loaded edge.

This paper expands previous research by using state-of-the-art solution techniques and composite modelling provided by Abaqus. It also provides guidelines and addresses common problems faced by analysts.

Acknowledgments

This paper was produced in the framework of the project *Structural joints for building frames of pultruded fibre reinforced polymers*. This research was supported by a Marie Curie Intra European Fellowship within the 7th European Community Framework Programme under contract grant PIEF-GA-2012-327142. The author would like to thank Dr. Paul Davidson and Professor Anthony Waas for providing raw data for the finite element modelling of the DCB test presented in this paper, and Professor Stephen Hallett for taking time to discuss some modelling issues.

References

1. Abaqus Manual (2013) Version 6.13 Dassault systems http://www.simulia.com
2. Lemaitre J (1986) Local approach of fracture. Eng Fract Mech 25:523-537
3. Schwarze M, Reese (2009) A reduced integration solid-shell finite element based on the EAS and the ANS concept – Geometrically linear problems. Int J Numer Meth Eng 806:1322-1355.
4. Parisch H (1995). A continuum-based shell theory for non-linear applications. Int J Numer Meth Eng 38:1855-1833
5. Hauptmann R, Schweizerhof K (1998) A systematic development of 'solid-shell' element formulations for linear and non-linear analyses employing only displacement degrees of freedom. Int J Numer Meth Eng 42:49–69

6. Hauptmann R, Schweizerhof K, Doll S (2000) Extension of the 'solid-shell' concept for application to large elastic and large elastoplastic deformations. Int J Numer Meth Eng 49:1121–1141
7. Remmers JC, Wells GN, de Borst R (2003) A solid-like shell element allowing for arbitrary delaminations. Int J Numer Meth Eng 58:1701-1736
8. Mi Y, Crisfield MA, Davies GAO, Hellweg HB (1998) Progressive delamination using interface elements. J Compos Mater 32(14):1246-1272
9. Petrossian Z, Wisnom MR (1998) Prediction of delamination initiation and growth from discontinuous plies using interface elements. Compos Part A – Appl S 29:503-515
10. Chen J, Crisfield M, Kinloch AJ, Busso EP, Matthews FL, Qiu Y (1999) Prediciting progressive delamination of composite material specimens via interface elements. Mech Compos Mater St 6:301-317
11. Alfano G, Crisfield MA (2001) Finite element interface models for the delamination analysis of laminated composites: mechanical and computational issues. Int J Numer Meth Eng 50:1701-1736
12. Borg R, Nilsson L, Simonsson K (2001) Simulation of delamination in fiber composites with a discrete cohesive failure model. Compos Sci Technol 61:667-677
13. Turon A (2006) Simulation of delamination in composites under quasi-static and fatigue loading using cohesive zone models. PhD thesis, Univ. Girona
14. Jiang WG, Hallett SR, Green BG, Wisnom MR (2007) A concise interface constitutive law for analysis of delamination and splitting in composite materials and its application to scaled noteched tensile specimens. Int J Numer Meth Eng 69:1982-1995
15. Wisnom MR (2010) Modelling discrete failures in composites with interface elements. Compos Part A – Appl S 41:795-805
16. Schellekens JCJ, de Borst R (1993) On the numerical integration of interface elements. Int J Numer Meth Eng 36:43-66
17. Hashin Z (1983) Analysis of composite materials. J Appl Mech 50:481-505
18. Jones RM (1999) Mechanics of composite materials, 2nd edition. Taylor and Francis, USA.
19. Nairn JA (2000) Matrix microcracking in composites. In: Kelly A, Zweben C (eds.) Comprehensive composite materials, Vol. 2, Elsevier Science, Amsterdam, Chapter 2.13, 433-528
20. Sims GD, Broughton WR (2000) Glass fiber reinforced plastics – Properties. In: Kelly A, Zweben C (eds.) Comprehensive composite materials, Vol. 2, Elsevier Science, Amsterdam, Chapter 2.05, 151-197

21. Pinho ST (2005) Modelling failure of laminated composites using physically-based failure models. PhD thesis, Imperial College London
22. Dugdale DS (1960) Yielding of steel sheets containing slits. J Mech Phys Solids 8:100-104
23. Barenblatt GI (1962) The mathematical theory of equilibrium cracks in brittle fracture. In: Dryden HL, von Kármán Th, Kuerti G, van den Dungen FH, Howarth L (eds.) Advances in Applied Mechanics, Vol. 7, 55-129
24. Tvergaard V, Hutchinson JW (1992) The relation between crack growth resistance and fracture process parameters in elastic-plastic solids. J Mech Phys Solids 40:1377–1397
25. Xu XP, Needleman A (1994) Numerical simulations of fast crack growth in brittle solids. J Mech Phys Solids 42(9):1397–1434
26. Camanho PP, Dávila CG, Moura MF (2003) Numerical simulation of mixed-mode progressive delamination in composite materials. J Compos Mater 37(16):1415-1438
27. Knops M (2008) Analysis of failure in fiber polymer laminates – the theory of Alfred Puck. Springer, Germany
28. Puck A, Schürmann H (2002) Failure analysis of FRP laminates by means of physically based phenomenological models. Compos Sci Technol 62:1633-1662
29. Tsai SW, Wu EM (1971) A general theory of strength for anisotropic materials. J Compos Mater 5(1):58–80
30. Hashin Z, Rottem A (1973) A fatigue failure criterion for fiber reinforced materials. Report AFOSR-TR-73-0686, Department of Materials Engineering, Technion, Israel Institute of Technology
31. Hashin Z (1980) Failure criteria for unidirectional fiber composites. J Appl Mech 47:329-334
32. Murray YD (1989) Theory and verification of the fiber composite damage model implemented in DYNA3D. Report DNA-TR-89-132
33. Barbero EJ (2010) Introduction to composite materials design, 2nd edition. CRC Press, Philadelphia, USA
34. Rastellini F, Oller S, Salomón O, Oñate E (2008) Composite materials non-linear modelling for long fibre-reinforced laminates – Computational basis, computational aspects and validations. Comput Struct 86(9):889-896
35. Martínez X, Oller S (2009) Numerical simulation of matrix reinforced composite materials subjected to compression loads. Arch Comput Methods Eng 16:357-397
36. Martínez X, Rastellini F, Oller S, Flores F, Oñate E (2011) Computationally optimized formulation for the simulation of composite materials and delamination failures. Compos Part B – Eng 42:134-144

37. Pérez MA, Martínez X, Oller S, Gil L, Rastellini F, Flores F (2013) Impact damage prediction in carbon fiber-reinforced laminated composite using the matrix-reinforced theory. Compos Struct 104:239-248
38. Ladeveze P, Le Dantec E (1992) Damage modelling of the elementary ply for laminated composites. Compos Sci Technol 43:257-267
39. Matzenmiller A, Lubliner J, Taylor RL (1995) A constitutive model for anisotropic damage in fiber-composites. Mech Mater 20:125-152
40. Lemaitre J (1996) A course on damage mechanics, 2nd edition. Springer-Verlag, Heidelberg, Germany
41. Lapczyk I, Hurtado JA (2007) Progressive damage modeling in fiber-reinforced materials. Compos Part A – Appl S 38:2333-2341
42. Maimí P, Camanho PP, Mayugo JA, Dávila CG (2007) A continuum damage model for composite laminates. Part I: constitutive model. Mech Mater 39:897-908
43. Flatscher Th, Pettermann HE (2011) A constitutive model for fiber-reinforced polymer plies accounting for plasticity and brittle damage including softening – Implementation for implicit FEM. Compos Struct 93:2241-2249
44. Lemaitre J, Dufailly J (1987) Damage measurements. Eng Fract Mech 28:643-661
45. Krajcinovic D (1989) Damage mechanics. Mech Mater 8:117-197
46. Ju JW (1990) Isotropic and anisotropic damage variables in continuum damage mechanics. J Eng Mech-ASCE 116(12):2764-2770
47. Catalanotti G, Camanho PP, Xavier J, Dávila CG, Marques AT (2010) Measurement of resistance curves in the longitudinal failure of composites using digital image correlation. Compos Sci Technol 70:1986-1993
48. Bažant ZP, Oh BH (1983) Crack band theory for fracture of concrete. Mater Struct 16:155-177
49. Allix O, Ladevèze P (1992) Interlaminar interface modelling for the prediction of delamination. Compos Struct 22(4):235-242
50. Falk ML, Needleman A, Rice JR (2001) A critical evaluation of cohesive zone models of dynamic fracture. J Phys IV, Proc 11(Pr.5):43–50
51. Bažant ZP, Jirásek M (2002) Nonlocal integral formulations of plasticity and damage: survey of progress. J Eng Mech-ASCE 128(11):1119-1149
52. Yang Q, Cox B (2005) Cohesive models for damage evolution in laminated composites. Int J Fract 133:107–37
53. Daudeville L, Allix O, Ladevèze P (1995) Delamination analysis by damage mechanics. Some applications. Compos Engng 5(1):17–24

54. Turon A, Dávila CG, Camanho PP, Costa J (2007) An engineering solution for mesh size effects in the simulation of delamination using cohesive zone models. Eng Fract Mech 74:1665-1682
55. Brewer JC, Lagace PA (1988) Quadratic stress criterion for initiation of delamination. J Compos Mater 22:1141-1155
56. Mohammadi S, Owen DRJ, Peric D (1998) A combined finite/discrete element algorithm for delamination analysis of composites. Finite Elem Anal Des 28:321-336
57. Benzeggagh ML, Kenane M (1996) Measurement of mixed-mode delamination fracture toughness of unidirectional glass/epoxy composites with mixed-mode bending apparatus. Compos Sci Technol 56:439-449
58. Harper PW, Hallett SR (2008) Cohesive zone length in numerical simulations of composite delamination. Eng Fract Mech 75:4774-4792
59. Bažant ZP, Planas J (1998) Fracture and size effect in concrete and other quasi-brittle materials. CRC Press, Boca Raton, USA
60. Belytschko T, Bažant ZP, Hyun YW, Chang TP (1986) Strain-softening materials and finite-element solutions. Comput Struct 23(2):163-180
61. Pijaudier-Cabot G, Bažant ZP (1987) Nonlocal damage theory. J Eng Mech-ASCE 113(10):1512-1533
62. Jirásek M, Patzák B (2001) Models for quasi-brittle failure: theoretical and computational aspects. Proceedings of the 2nd European Conference on computational mechanics; solids, structures and coupled problems in engineering, 70-71 (full paper on CD Rom)
63. Needleman A (1988) Material rate dependence and mesh sensitivity in localization problems. Comput Method Appl M 67:69-85
64. Maimí P, Camanho PP, Mayugo JA, Dávila CG (2007) A continuum damage model for composite laminates. Part II: computational implementation and validation. Mech Mater 39:909-919
65. Chaboche JL, Feyel F, Monerie Y (2001) Interface debonding models: a viscous regularization with a limited rate dependency. Int J Solids Struct 38:3127-3160
66. Gao YF, Bower AF (2004) A simple technique for avoiding convergence problems in finite element simulations of crack nucleation and growth on cohesive interfaces. Model Simul Mater Sc 12:453-463
67. Hamitouche L, Tarfaoui M, Vautrin A (2008) An interface debonding law subject to viscous regularization for avoiding instability: application to the delamination problems. Eng Fract Mech 75:3084-3100

68. Crisfield M (1997) Non-linear finite element analysis of solids and structures, Volume 1 – Essentials. John Wiley & Sons Ltd., Chichester, UK
69. Davidson P, Waas AW (2012) Non-smooth mode I fracture of fibre-reinforced composites: an experimental, numerical and analytical study. Phil Trans R Soc A 370:1942-1965
70. ASTM International 2001. ASTM D 6671 – 01: Standard test method for mixed mode I-mode II interlaminar fracture toughness of unidirectional fiber reinforced polymer matrix composites, USA
71. Reeder JR, Demarco K, Whitley KS (2004) The use of doubler reinforcement in delamination toughness testing. Compos Part A – Appl S 35:1337-1344
72. Gustafson PA, Waas AW (2009) The influence of adhesive constitutive parameters in cohesive zone finite element models of adhesively bonded joints. Int J Solids Struct 46:2201-2215
73. Spearing SM, Beaumont PWR (1992) Fatigue damage mechanics of composite materials. I: Experimental measurement of damage and post-fatigue properties. Compos Sci Technol 44:159-168
74. Wisnom MR, Chang FK (2000) Modelling of splitting and delamination in notched cross-ply laminates. Compos Sci Technol 60:2849-2856
75. van der Meer FP, Oliver C, Sluys LJ (2010) Computational analysis of progressive failure in a notched laminate including shear nonlinearity and fiber failure. Compos Sci Technol 70:692-700
76. Hallett SR, Wisnom MR (2006) Numerical investigation of progressive damage and the effect of layup in notched tensile tests. J Compos Mater 40(14):1229-1245
77. Yashiro S, Okabe T, Toyama N, Takeda N (2007) Monitoring damage in holed CFRP laminates using embedded chirped FBG sensors. Int J Solids Struct 44:603-613
78. van der Meer FP, Sluys LJ (2009) Continuum models for the analysis of progressive failure in composite laminates. J Compos Mater 43(20):2131-2156
79. Hancox NL, Mayer NL (1994) Design data for reinforced plastics: a guide for engineers and designers. Chapman & Hall, London, UK
80. Pinho ST, Robinson P, Iannucci L (2006) Fracture toughness of the tensile and compressive fibre failure modes in laminated composites. Compos Sci Technol 66:2069-2079
81. van der Meer FP (2010) Computational modeling of failure in composite laminates. PhD thesis, Delft Univ. Tech.
82. Hallett SR, Wisnom MR (2006) Experimental investigation of progressive damage and the effect of layup in notched tensile tests. J Compos Mater 40(2):119-141
83. Finite element guidelines for simulation of fibre-tension dominated failures in composite materials validated by case studies. Compos Struct (under review)